Biochimica et Biophysica Acta, 559 (1979) 153–208

BBA 85194

APPLICATION OF LASER RAMAN AND INFRARED SPECTROSCOPY TO THE ANALYSIS OF MEMBRANE STRUCTURE

DONALD F.H. WALLACH *, SURENDRA P. VERMA and JEFFREY FOOKSON

Tufts-New England Medical Center, Therapeutic Radiology Department, Radiobiology Division, 171 Harrison Avenue, Boston, MA 02111 (U.S.A.)

(Received October 3rd, 1978)

Contents

* To whom correspondence should be addressed.

I. Introduction

Raman spectroscopy and infrared absorption spectroscopy are two methods that are largely complementary. Raman scattering signals and infrared absorption bands derive from similar types of molecular motions, i.e. bond and lattice vibrations or rotations. However, many molecular modes that yield weak Raman signals show intense infrared absorption and conversely. In particular, polar groups produce large infrared signals, with the intensity of an absorption band proportional to the size of the local dipole moment modulation resulting from the molecular motion. Raman signals, proportional to the local polarisability fluctuations, arise primarily from covalent motions. As an example, infrared spectroscopy should yield insights into the structure of membrane lipid head groups, their hydration behavior and the lattice dynamics of membrane components, whereas Raman spectroscopy would be more informative about processes that occur within the membrane core. General introductions to infrared and laser Raman spectroscopy are found in Refs. 1 and 2 and this article will concentrate on recent progress in the area of membrane Raman and infrared spectroscopy.

Raman spectroscopy has proven itself a versatile tool for the measurement of hydrocarbon chain configurations and interactions in systems consisting of monoglycerides [3] saturated, unsaturated and deuterated fatty acids (e.g. Refs. 4–7), saturated and unsaturated lecithins (e.g. Refs. 4–17), with and without cholesterol, and other phospholipids (3), phospholipid-peptide and phospholipid-protein combinations [17–22], plasma membranes of eukaryotic cells [23–30], sarcoplasmic reticulum [31], photoreceptor membrane proteins [32] and systems containing conjugated polyenes [25,33]. Raman spectroscopy has also provided important information about the proteins of biomembranes and their interactions with membrane lipids [23–32,34].

In this article we will focus on how Raman spectroscopy has extended our knowledge of biomembrane structure. However, before this we will comment on technical aspects and on some relevant model systems.

II. Raman spectroscopy – Technical

IIA. Conventional scanning Raman spectroscopy

IIA (1). Standard technique

Raman spectra are routinely obtained on samples (approx. 50 μl; 10 mg/ml) sealed into Kimex capillaries (approx. 0.9 mm ID). After sealing, these capillaries are placed in a temperature control device (e.g., Harney-Miller cell). The temperature is monitored by a telethermometer and regulated by a flow of cold or warm nitrogen. Temperature control is checked by determining transition temperatures of authentic lipids (dimyristoyl phosphatidylcholine; dipalmitoyl phosphatidylcholine; octadecane) in the laser beam. Local heating due to the laser beam is about 2.5°C.

A simple computer-assisted recording technique, used in our laboratory, for complicated systems such as biomembranes, is described in the following.

Raman spectra are recorded with a Ramalog 4 Raman spectrometer (Spex Industries, Metuchen, NJ, U.S.A.) interfaced to an Interdata (Model 70) computer. An Ar^+ laser (Spectra Physics model 164), usually tuned at 488 nm, is used as an excitation source. For spectra at low frequencies an interference filter is used to block plasma lines. With solid (crystalline) materials and concentrated liposomes slits are set at 50 μM (resolution

approx. 1 cm^{-1}) and excited at 800 mW power. With membranes 300 mW power (slits 200 μm) is used, except for resonance Raman spectroscopy, where 50 mW is employed. Raman scattering at right angles to the laser beam is detected by a thermoelectrically-cooled photomultiplier (RCA 31034) and is recorded in terms of photons/s. The 'dark' rates of the photo cell are 7–10 counts per s vs. Raman scattering from samples in the order of 10^3–10^5/s. Scanning is done through the computer (loaded with the VIE8D Ramancomp Computer Program, Spex Industries). The following specifications are typical for scanning: (i) maximum time and minimum time for each data point, 1.5 and 0.5 s, respectively (longer with smaller slits), except for resonance Raman spectroscopy where 0.5 and 0.1 s, respectively, are used; (ii) photon counts 10^4–10^5 maximum and 100 minimum. Scanning is in steps of one wave number. Scans are incremental between data points and no counts are recorded between data points. Photon counts are stored in the computer memory during scanning (1–4 scans; approx. 300) and the stored spectra, when appropriate, are averaged and smoothed by a least-squares procedure (included in the computer program), ultimately plotted on the Ramalog recorder using appropriate background suppressions and scale expansions. To accurately determine the positions of some bands, first- and second-derivative spectra are computed and recorded. Also, to measure integrated intensities, areas under scattering peaks can be computed when necessary. Raman spectra, which were stored in the computer memory can be added, subtracted, or multiplied.

To determine the change of Raman scattering with temperature, the following procedure is employed: the samples, in position but with the laser beam occluded, are equilibrated for 20 min at the desired temperature. Samples are then equilibrated a further 5 min in the laser beam before scanning the appropriate region (1–4 scans). During equilibration at the subsequent temperature the (averaged, smoothed) spectra are plotted. The procedure for the ≈1527 and ≈1158 cm^{-1} bands of conjugated polyenes is identical except that the 5-min equilibration in the laser beam is omitted and scanning is from 1400 to 1600 cm^{-1} and 1000 to 1200 cm^{-1}, respectively (maximum 100s/scan for each band). Scattering vs. temperature curves are obtained going both from low to high temperatures and vice versa. Scans are conducted in triplicate. To determine effects of pH, Ca^{2+} and other external variables, individual measure points are examined in triplicate.

Scattering intensities are expressed by reference to internal standards. Generally, the ≈2850 cm^{-1} CH-stretching band and 722 cm^{-1} (CH-stretching of choline) can serve as reliable internal standards.

Another reference line suitable for the study of thermal variations is the SO_4 stretching band at 982 cm^{-1}. However, one must exclude possible variations in this band due to changes in binding such as occur during unfolding of ribonuclease [35].

When examining the CH-stretching region of materials in aqueous solution or dispersion, one must correct for the low frequency tail of the strong CH-stretching band (peaks at 3439 cm^{-1} in liquid water and 3220 cm^{-1} in ice I). Indeed, without such correction, the change in water background in going from liquid water to ice I during thermal studies, can prevent evaluation of the CH-stretching region. Two approaches are useful.

The first is as follows: a water spectrum is recorded, between 2800 and 3400 cm^{-1} for the temperature at which the sample is examined. This spectrum is stored in the computer. The sample is then scanned at the same temperature over the same frequency range. The spectrum is stored and normalized, using the water (ice) peaks, to correct for the lesser water content of the sample. The water (ice) spectrum is then subtracted from the sample spectrum and plotted.

The second approach involves the replacement of H_2O by ^2H_2O. For a 10% sample concentration, 50 % $H_2O/^2H_2O$ mixtures appear satisfactory.

When samples are frozen rapidly (not the usual procedure) the intense Rayleigh scattering of the incident laser beam produces Raman scattering from the wall of the sample capillary. This leads to a prominent band at 935 cm^{-1} and a somewhat weaker one at 900 cm^{-1}. The Rayleigh scattering of some membrane preparations, e.g. membrane vesicles may also suffice, even above freezing, to excite Raman scattering from the capillary. These are spurious peaks which may be removed by optical filters. It is also feasible to subtract the capillary wall-spectrum, by the computer, from the sample spectrum.

IIA (2). Use of a 'third monochromator'

The detection of low frequency Raman spectra is limited by the ability of the spectrometer to discriminate against laser light, i.e. Tyndall or Rayleigh scattering from the sample. The problem is particularly acute in the case of turbid or opalescent biological materials, for which it is usually not possible to obtain spectra (with a conventional dual monochromator) closer than 100–150 cm^{-1} to the exciting wavelength, even though the stray light transmitted by the monochromator at 100 cm^{-1} from the laser frequency is decreased by 10^{-10} from its peak height. Of the various schemes devised to improve the rejection of stray light, the addition of a 'third monochromator' following the exit slit of the spectrometer is the most versatile, economical and dependable [36]. It requires neither single-mode operation of the laser, nor operation at a specific wavelength, as does the technique of absorbing the Rayleigh scattered light with an iodine vapor cell. It does not limit spectrometer throughput significantly as do techniques involving interference filters nor does it require a stable interferometer. Typically, the addition of the third grating reduces stray-light by about 10^3 and permits the recording of the spectra from water-free samples to within a few wavenumbers of the laser frequency *.

IIA (3). Derivative spectroscopy

Genzel et al. [37] and Genzel and Martin (personal communication) show that a 'third monochromator' cannot, in the case of water-containing samples, effectively reduce the strong background in the low frequency region, due to inelastic light scattering by water. This scattering arises largely from the reorientation of water molecules whose polarisability is anisotropic. Due to their small dimension, water molecules reorient rapidly enough to produce anisotropy scattering up to $\Delta cm^{-1} \approx 50$. Because of the high water content of most membrane samples, this background is large. Because the background is large, slow fluctuations in background – due to thermal gradients produced by the laser beam – can simulate Raman bands.

According to Genzel and Martin (personal communication), of the methods described by Genzel et al. [37], only the differentiation system of Yacoby and Linz [38] has proven consistently reliable in adequately reducing background due to inelastic light-scattering from water. In this approach the background contribution is reduced by directly obtaining the derivative of scattered intensity with respect to energy displace-

* The third monochromator is used as a stray-light filter only for the low frequency region. For higher frequencies it can be slaved to the double spectrometer to eliminate grating ghosts. A high throughput mirror operation is also available when stray-light is not a problem.

ment, dI/du. The recorded signal is then [38]:

$$I(t) = [1 + f(t)]\,[(dI_{RS}/du) \pm (dI_{RB}/du)]$$

where I_{RB} denotes background scattering intensity, I_{RS} denotes Raman signal intensity and $f(t)$ describes the random fluctuations in intensity arising from thermal gradients.

Since I_{RB} varies less with frequency than I_{RS}, the noise associated with $(dI_{RB}/du)f(t)$ is reduced relative to the signal.

Numerical differentiation (such as can be achieved by computer) is insufficiently accurate for the problem at hand and it is also too noisy. The real-time method of Yacoby and Linz [38] in contrast appears simple and efficient. Here, differentiation is achieved by vibrating a glass plate near the exit slit of the 'third monochromator' to produce an optical frequency peak-to-peak variation of 3 cm^{-1} at 14.5 Hz in the spectrometer output. The glass plate assembly is attached to the cone of a loudspeaker. This is driven, via an audio power amplifier, by the reference oscillator of a lock-in amplifier. The detector signal is fed into the lock-in amplifier and recorded (bypassing the electronic path used for other spectral regions).

IIA (4). Use of a tunable dye laser

Raman analyses of some biomembranes are complicated by luminescence, which can hinder quantitative intensity measurements particularly in the CH-stretching, and amide I and CH-deformation regions.

We believe that it is the membrane proteins that are the source of this background because (a) we do not encounter the problem with purified lipids, and (b) severe luminescence is common with numerous highly purified proteins.

We believe that the most likely source of luminescence with membranes and protein lacking obvious visible fluorophores involves phosphorescence as well as fluorescence because the luminescence decays somewhat slowly ($t_{1/2} \approx 1$ ms). The phenomenon is enhanced by temperature-reduction and the luminescence can be suppressed somewhat more readily by quenchers of excited triplet states (e.g. paramagnetic cations) than by singlet-state quenchers.

The luminescence is particularly problematic for the following reasons:

(a) The background varies strongly with Δcm^{-1} in certain regions, e.g. with 488 nm excitation, the slope of luminescence of dry protein, drops sharply with increasing or decreasing wavenumber above 2700 cm^{-1} or below 1900 cm^{-1}.

(b) Luminescence varies with time of exposure, generally increasing initially. It can be 'bleached' by prolonged exposure.

(c) Luminescence increases with decreasing temperature. This effect is sufficiently severe to complicate analysis of the CH-stretching region of some proteins and many biomembranes at temperatures less than $-5°C$.

(d) In some samples the position of the luminescence band varies with hydration.

A number of approaches have been employed to eliminate interference by luminescence. For example, it is conventional to suppress luminescence by 'burning it off'. This approach is not permissible with biologically active samples. Indeed, the presence of luminescence implies localized sample heating, which should be avoided.

The use of quenching agents is also not acceptable, since to be efficient, these must be used at levels where they are biologically active. This approach also does not avoid sample heating.

Gating approaches offer no advantages, particularly since the decay of any fluorescent

component is too rapid for anything but pulsed laser operation with appropriate circuitry. First, such approaches are prohibitively costly and not well tested. Second, they would not avoid localized heating. Manipulations such as Fourier transformation have equivalent disadvantages.

A useful solution to the problem (and also the most economical one) may be to use an ion-argon laser to pump a tunable dye laser and to use the latter as exciting source.

IIB. Multiplex Raman spectroscopy

Raman spectra are classically recorded using a scanning monochromator, photomultiplier-detector, and a photon-counting system, commonly in line with a small computer. Particularly from the viewpoint of biological experimentation, however, such single channel scanning has two major disadvantages, namely:

(a) Data acquisition is very time consuming, seriously restricting the number of experiments that can be performed, i.e. limiting the information that can be extracted from precious biological samples.

(b) Laser light-induced sample modification (or deterioration) during data acquisition is an ever-present problem, requiring otherwise unnecessary control studies.

An alternative method of Raman data acquisition is multichannel spectrum detection, using direct reading intensified Vidicon systems as pioneered particularly by Bridoux and Delhaye [39]. As opposed to scanning methods which record only one resolution element at a time, multichannel (multiplex) systems analyze a broad spectral region in parallel, yielding time gains proportional to the number of resolution elements in the broad bandpass. In a video system the dispersed spectrometer output is imaged on a Vidicon, and the output is processed by video techniques. The image spectrum is sampled at the video frame rate, with the integrated intensity along each raster line corresponding to one data point.

The multichannel approach thus offers an enormous advantage in speed. The full advantage (the capacity to record a full spectral interval at the speed of photoelectric detection) corresponds to an increase in speed equal to the spectral interval divided by the resolution.

III. Spectral regions useful for membrane studies

IIIA. The CH-stretching (2700–3100 cm^{-1}) and CH-bending (1400–1500 cm^{-1}) regions

IIIA (1). Methylene CH-stretching

Diverse membranes yield prominent Raman scattering bands in the CH-stretching region, due primarily to the CH-stretching vibrations of CH_2 and CH_3 residues. In lipids with crystalline saturated fatty acid chains (Fig. 1) the band near 2850 cm^{-1} and the sharp line near 2880 cm^{-1} are most reasonably attributed to symmetric and asymmetric methylenic CH_2-stretching of polymethylenic segments respectively [5,11,15]. However, the spectra of solid, deuterated derivatives of stearic acid indicate that the CH-stretching vibrations of CH_2 groups in long methylenic segments are not representative of (a) CH_2 residues adjacent to the CH_3 terminus, or (b) CH_2 residues adjacent to the carboxyl residue. The latter give rise to a feature at 2920 cm^{-1} [5]. Asymmetric CH-stretching of CH_3 gives a band near 2964 cm^{-1} (for the in skeletal plane mode) and near 2952 cm^{-1} (for the out of plane mode). Symmetric methyl CH-stretching occurs between 2928

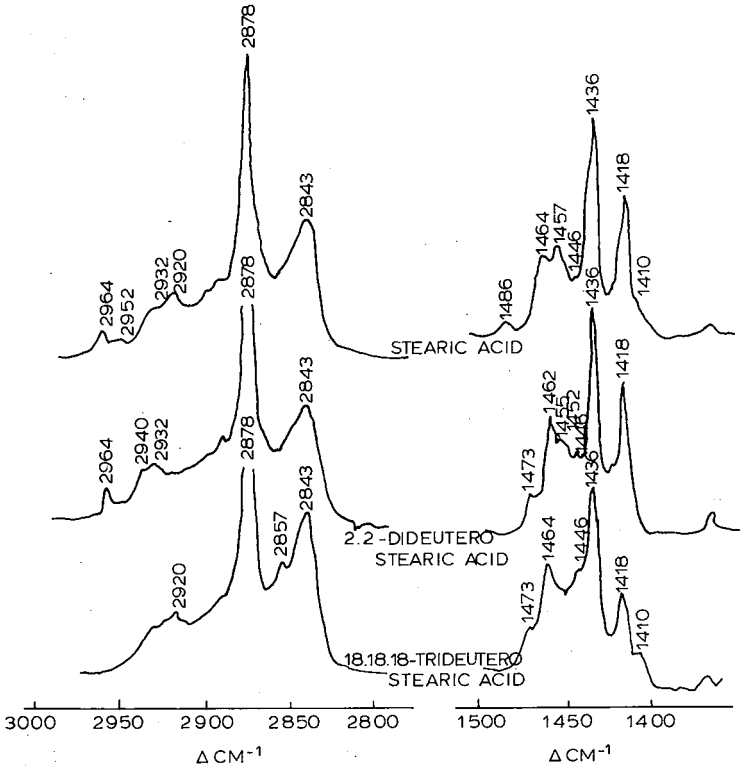

Fig. 1. Raman spectra of solid stearic acid, 2,2-dideuterostearic acid, and 18,18,18-trideuterostearic acid in the CH-stretching region (left: 2800–3000 cm^{-1}) and the HCH-deformation range (right: 1400–1500 cm^{-1}). Recorded at 22°C. From Ref. 5.

and 2945 cm^{-1}. However, since methyl deuteration merely reduces, but does not abolish scattering in this region, it must contain methylene contributions also. This is relevant to intensity changes near 2935 cm^{-1} (see Section IIIA (3)).

Unsaturated fatty acids (below their melting points (Fig. 2)) exhibit much more complex banding in the CH-stretching region. This is compatible with non-equivalence of CH_2-residues, in particular those adjacent to one or two –HC=CH bonds, or a HC=CH bond and a CH_3-terminus. However, interactions between CH-stretching fundamentals and HCH-deformation overtones may also be involved. We will address this last issue below.

The CH-stretching modes of strong (100 kcal/mol) CH-bonds are due almost entirely to hydrogen motion and highly localized. In contrast to the skeletal vibrations at lower frequencies, CH-stretching bands should therefore be quite insensitive to chain configuration or environment. However, this is not the case, as is obvious from the spectra of solid unsaturated fatty acids. Moreover, the relative intensities of bands comprising the CH-stretching region and, to some extent, the frequencies of these features, reflect the state of biomembrane acyl chains and, as shown below, can accurately monitor cooperative state-transitions, whether induced by a small temperature shift, or by subtle changes in proton concentration. This circumstance is most reasonably explained by the proposal originally submitted by Schachtschneider and Snyder [40], that the structure of the

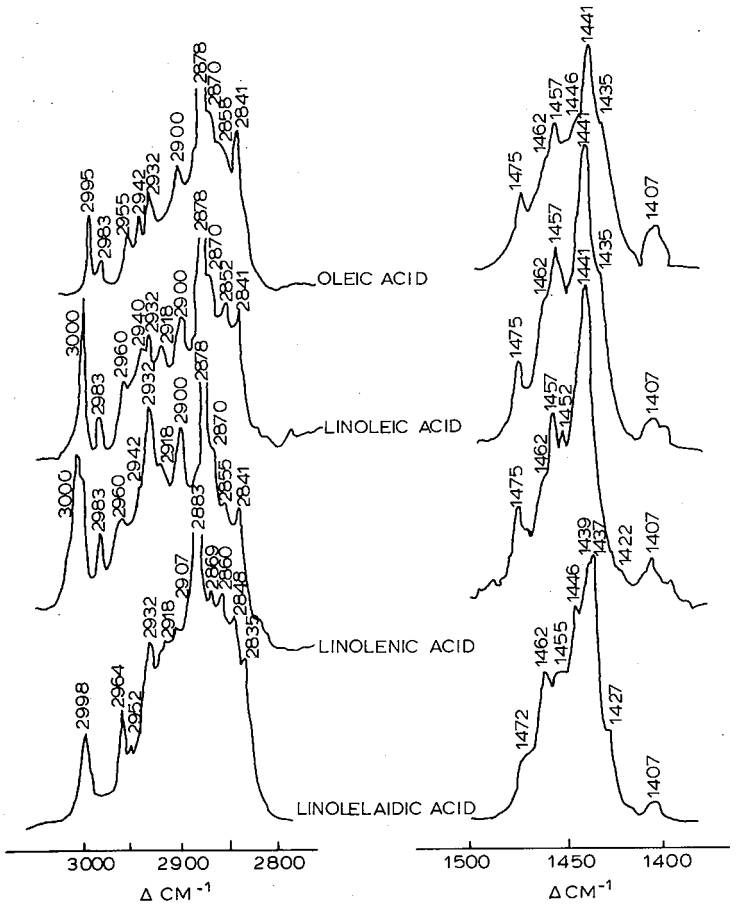

Fig. 2. Raman spectra of solid oleic, linoleic, linolenic and linolelaidic acids in the CH-stretching region (left: 2800–3100 cm^{-1}) and the HCH-deformation region (right: 1400–1500 cm^{-1}). Recorded at −40°C. From Ref. 5.

CH-stretching region depends upon the interactions, enhanced by Fermi resonance, of CH-stretching fundamentals with HCH-deformation overtones. HCH-deformation vibrations vary prominently with chain configuration and resonance enhancement depends markedly on the overlap integral of overtones and fundamentals (of the same vibrational symmetry). Therefore, unobtrusive modifications in the HCH-deformation region can be expected to be amplified by resonance interactions.

A recent analysis by Snyder et al. [41] on Raman spectra in the CH-stretching regions of extended polymethylene chains shows that the narrow ≈2880 cm^{-1} feature is due to asymmetric CH_2 CH-stretching and the somewhat broader band(s) near 2850 cm^{-1} to symmetric CH-stretching of CH_2 groups. These assignments are as before. However, they show that the ≈2850 cm^{-1} region is sensitive to chain packing and demonstrate a single broad band, at 2846 cm^{-1}, for orthorhombic structures, two broad maxima, at 2846 and 2855 cm^{-1}, for triclinic crystals and a single narrow line at 2846 cm^{-1}, for hexagonal crystal structures. (All exhibit a single narrow feature at 2879 cm^{-1}.) Extensive complexities in the ≈2850 cm^{-1} region are also observed with various solid unsaturated fatty acids,

although the feature at ≈2880 cm^{-1} is pronounced and sharp in all cases [5]. Finally, Snyder et al. [41] demonstrate that a broad, asymmetric band underlies the ≈2880 feature and extends to about 2990 cm^{-1}.

Snyder et al. [41] attribute the complexity of the CH-stretching region of hydrocarbon chains to Fermi resonance interactions involving binary combinations between methylene bending modes (fundamentals 1443–1467 cm^{-1} in their case) and the symmetric methylenic CH-stretching mode. The asymmetric mode, near 2890 cm^{-1} is forbidden by symmetry from participating in Fermi resonance interactions and is thus not sensitive to changes in chain environment. However the strong Fermi resonance interactions between symmetric CH-stretching fundamentals and appropriate binary combinations involving methylene bending modes produce 'broad, often strong secondary maxima, including the band underlying the sharp band at ≈2880 cm^{-1}. The breadth of the secondary maxima is attributed to the existence of a 'virtual continuum' of binary combination states and not just those few (zone center) which are normally invoked. Snyder et al. [41] further stress the 'density of binary states' which clearly depends on chain packing. They further point out that the Fermi interactions can be both intramolecular and intermolecular, the latter being dependent on chain packing and/or environment. Pronounced environmentally-induced changes in the 2880–2890 cm^{-1} region (see below) are ascribed to altered Fermi resonance interactions, between symmetric modes and not the modifications of asymmetric methylene CH-stretching.

We have also invoked Fermi resonance in our interpretation of the CH-stretching spectra of various fatty acids [5]. In solid stearic acid the CH-deformation region is characterized by a number of sharp bands the most prominent of which are at 1436 and 1418 cm^{-1} (Fig. 1). The complex banding in this region observed with C_{18} fatty acids vs. that observed with C_{36} polymethylenes [41] has not been fully explained. However, comparisons of stearic acid with [^{2}H]stearic acids allow some conclusions. Thus solid stearic acid yields discrete Raman scattering bands at 1418, 1436, 1457, 1464 and 1486 cm^{-1}, as well as shoulders at 1410 and 1446 cm^{-1}. The 1457 cm^{-1} feature is lacking in the spectrum of 18,18,18-trideuterostearic acid and is replaced by a band at 1455 cm^{-1} of equivalent relative intensity in 2,2-dideuterostearic acid. The 1486 cm^{-1} band is missing in both deuterated derivatives. In addition, the relative intensity of the 1418 cm^{-1} band of 18,18,18-trideuterostearic acid is less than that found with native stearic acid. ($[I_{1418}/I_{1436}] = 0.45$ for 18,18,18-trideuterostearic acid, vs. 0.66 for stearic acid). 2,2-Dideuterostearic acid gives bands at 1418, 1436, 1446, 1455, 1462 and 1473 cm^{-1}, as well as a shoulder at 1452 cm^{-1}. However, the 1410 cm^{-1} shoulder is not observed with this compound, suggesting it arises from methylene residues proximal to carboxyl residues. These data as well as the computed intensities of the variable peaks, relative to the major, common methylene feature at 1436 cm^{-1}, indicate that the band at 1455–1457 cm^{-1} arises from methyl HCH-deformation modes. The other bands appear to comprise overlapping signals from methyl and methylene groups, with a major contribution from methylene-deformation at 1418 cm^{-1}. The broadness of the feature at 1462–1465 cm^{-1} of stearic acid, vs. that of 18,18,18-trideuterostearic acid is probably also due to overlapping methyl and methylene contributions (asymmetric deformation and scissoring respectively), which are eliminated when the methyl terminus is deuterated.

In the liquid stearic acid, the HCH-deformation region reduces to a single broad band, with an increase in relative intensity between 1460 and 1440 cm^{-1}. Concomitantly, the CH-stretching region also becomes diffuse, with replacement of the sharp 2878 cm^{-1} feature by a broad band at approx. 2890 cm^{-1}, emergence of a second broad feature at

approx. 2926 cm^{-1}, but a narrowing of the 2843 cm^{-1} feature of the solid and a shift of this peak to 2850 cm^{-1} (Fig. 3). Our explanation for the changes in the 2843–2850 cm^{-1} band is that they represent a loss of, or reduced interaction with the overtone of a symmetric methylene bending component contributing to the 1418 cm^{-1} feature of solid stearic acid. The broadening as well as the shift of the 2880–2890 cm^{-1} are considered secondary to the diffuseness of the HCH-deformation band and its greater relative intensity at approx. 1450 cm^{-1}: the processes responsible for these changes in the deformation region would repeat in the harmonics occurring in the CH-stretching region, leading to the diffuse, frequency-shifted pattern observed between 2880 and 3000 cm^{-1}, which is in its main features similar to the patterns observed with liquid-crystalline phases. The emergence, in the liquid state, of the prominent feature at approx. 2926 cm^{-1} cannot be attributed exclusively to CH_3-stretching or CH-stretching of CH_2 residues adjacent to carboxyls, since it is equally prominent in stearic acid and the two deuterated derivatives [5]. Enhancement in this region might be expected, however, from the broadening and intensity shifts in the HCH-deformation region.

The differences in the 1400–1500 cm^{-1} region, between solid, saturated and unsaturated C_{18} acids, as well as the distinctions between the various unsaturated acids, vividly demonstrate the great sensitivity of HCH-deformation modes to lipid chain architecture. This sensitivity, and the non-equivalence of CH_2-residues in unsaturated chains assuredly contributes to the great complexity of the CH-stretching regions of solid unsaturated fatty acids, as well as to the different scattering patterns found with increasing unsaturation, or *trans* vs. *cis* unsaturation [5].

IIIA (2). Intensity changes of methylene CH-stretching

Concerning the changes of lipid state that manifest themselves in the CH-stretching region, the intensity ratio, r, $[I_{\approx 2890}/I_{\approx 2850}]$ has proven extremely useful. In this ratio, the intensity of the 2850 cm^{-1} serves as 'internal standard'. That this can be permissible is suggested by Gaber and Peticolas [15]. These authors prepared mixtures of hexadecane and perdeuterohexadecane in various proportions and showed that the intensities of the C^2H-stretching band at 2106 cm^{-1} and the CH-stretching band at 2850 cm^{-1} were both

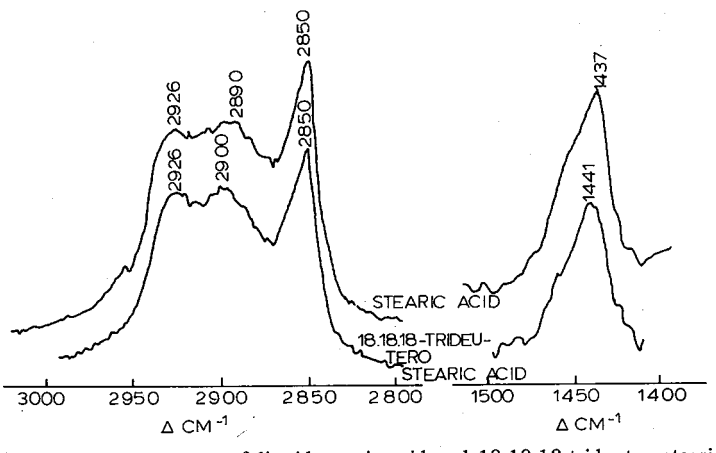

Fig. 3. Raman spectra of liquid stearic acid and 18,18,18-trideuterostearic acid in the CH-stretching region (left: 2800–3100 cm^{-1}) and the HCH-deformation region (right: 1400–1500 cm^{-1}). Recorded at 75–80°C. From Ref. 5.

exactly proportional to the mol fractions (over a range of 0–1.0) of the two compounds. However, $I_{\approx 2850}$ will not be constant for all chain packing situations and the width of the ≈2850 cm^{-1} band can also vary depending on chain packing. The ratio, r, for solid phospholipids ranges from 2.8 for distearoyl phosphatidylcholine to 2.2 for dipalmitoyl phosphatidylcholine, to 1.6 for dimyristoyl phosphatidylcholine. The value for dipalmitoyl phosphatidylcholine in solution is about 0.7, and in the case of aqueous phospholipid dispersions is much lower when these consist of unilamellar vesicles rather than multilamellar dispersions (e.g. ≈1.06 for vesicles of dimyristoyl phosphatidylcholine).

Gaber and Peticolas [15] have explored the basis for the changes in the CH-stretching region that occur with lipid phase transitions. They measured r for solid hexadecane in a matrix of perdeuterohexadecane at various mol fractions of the two compounds. Such isotopic mixtures have the same crystal lattice structure as the deuterated and undeuterated derivatives but cannot have the same vibrational interactions (C^2H vs. CH). Gaber and Peticolas [15] found that r decreased from a maximum of 2.20 to a value of about 1.45 at limiting levels of perdeuterohexadecane. This last value is still much higher than the one found with liquid hexadecane or the lipid chains in organic solution, i.e. about 0.70. Gaber and Peticolas [15] argue that the decrement from 2.20 to 1.45 (about 50% of what is found in going from solid to liquid hydrocarbon chains) is due to a destruction of interactions between the CH bending modes of vicinal lipid chains when H is replaced by ^2H. The change in intensity in the CH-stretching region is attributed to Fermi resonance between the first overtone of the ≈1450 cm^{-1} bending band and the degenerate CH_2-stretching band at ≈2890 cm^{-1}: when interchain coupling is destroyed by deuteration so are Fermi resonance effects that depend on this. To explain the further decrease in r to 0.7, a change that is associated by a 10 cm^{-1} increase in frequency of the ≈2890 cm^{-1} band, Gaber and Peticolas [15] invoke 'rotamer broadening': in the solid state the lipid chains constitute one (all *trans*) species. However, in the liquid state multiple rotameric forms (each with 1 line) can be expected. The I value of the liquid state is 'residual'. I_{total} is therefore considered to consist of three contributions: $I_{tot} = I_{lat} + I_{rot} + I_{resid}$. I_{lat} corresponds to the contribution of interchain interactions.

The argument for 'rotamer broadening' [15] is not really at variance with our view [5] as expressed above, that the broadening and frequency shift seen with lipid order-disorder transitions is also due to Fermi resonance effects. Moreover, the careful analysis of Snyder et al. [41] shows that Fermi resonance effects involve not only the centers of participating bands and that a 'continuum of binary states' can exist that lead to broad secondary bands. They also demonstrate that the shapes of the CH-stretching bands will depend strongly on the bending-mode fundamental and that Fermi resonance interactions are greater in the case of packed chains. Because of this the CH-stretching region is sensitive not only to order ⇌ disorder transitions but also to the nature of the order, i.e. crystal packing. According to Snyder et al. [41], $I_{\approx 2890}$ consists of approximately equal contributions from asymmetric methylene CH-stretching and symmetric methylene CH-stretching: the dependence of r on packing is a result of changes in the contribution of symmetric methylene CH-stretching, while asymmetric methylene CH-stretching remains nearly constant. However, in the liquid state, where there is conformation-disorder the ≈2880 cm^{-1} band consists primarily of asymmetric methylene CH-stretching with only a small contribution from symmetric methylene CH-stretching.

Gaber and Peticolas [15] show that $[I_{\approx 2890}/I_{\approx 2850}]$ is sensitive to (a) lateral (environmental) effects on extended chains, and (b) chain configuration. They propose a lateral

'order parameter', S_{lat}, defined in terms of the ratio r, $[I_{\approx 2890}/I_{\approx 2850}]$ as follows:

$$S_{lat} = \frac{r - 0.7}{1.5}$$

so that $S_{lat} = 1$ for a chain in the crystal state ($r = 2.2$) and $S = 0$ for chains in the liquid state ($r = 0.7$). Intermediate values are expected (and found) for other cases.

It should be noted however, that only the ratio of peak heights (not integrated intensities) will be environmentally sensitive [41]. Also r is a hybrid quantity because the intensities at both ≈2890 and ≈2850 cm^{-1} originate from multiple vibrational modes, as is obvious with unsaturated acyl chains. The value of S_{lat} lies, therefore, in monitoring the effect of specific environmental variables on given membrane systems.

As an alternative to using peak height changes to follow state transitions, Mendelsohn et al. [13] have used the increasing C^2H-stretching linewidth of phosphatidylcholine liposomes doped with deuterated stearate, to follow a shift to chain disorder. The same approach has been applied to the 2880–2890 cm^{-1} band of biomembranes by Verma et al. [29].

IIIA (3). Methyl CH-stretching

Whereas the character of the methylene CH-stretching signals has been extensively clarified, much less information exists for CH_3 signals, which dominate in protein-containing systems. Thus, Verma and Wallach [42] have shown that thermally-induced unfolding of ribonuclease at low pH (e.g. 2.72) produces a large increase of Raman scattering intensity of the 2930 cm^{-1} CH_3 stretching band relative to the intensity of a thermally stable internal standard. A plot of the intensity at 2930 cm^{-1} vs. temperature revealed a broad transition between 26 and 44°C which corresponds in position and width to the transition detected at this pH by differential thermal calorimetry, with the midpoint of the transition occurring at 38°C.

Thermodynamic analyses by Brandts and Hunt [43] indicate that the enthalpy changes occurring during ribonuclease unfolding are due to the exposure of apolar residues to water. Also, Larsson and Rand [3] proposed that Raman-active CH-stretching vibrations vary with solvent polarity and model experiments with methanol, dimethylsulfoxide and *tert*-butanol, as pure solvents and mixtures with H_2O or ^2H_2O [42] are consistent with these findings, revealing considerable modifications in the 2930 cm^{-1} region with polarity. However, many questions remain since poly-L-lysine, which completely lacks CH_3 residues, gives strong Raman scattering in the region under discussion.

IIIA (4). Conclusion

What is quite clear from these recent model and theoretical studies is that the CH-stretching region of the Raman spectrum will sensitively reflect vibrational interactions between membrane lipid acyl chains, as well as perturbations of such lateral effects. A perturbation already illustrated is chain isolation by isotopic dilution. Biologically more relevant perturbations would be found with (a) chain mixtures, (b) cholesterol-phospholipid systems, and (c) proteins-peptide intercalated into the hydrocarbon phase. Some of these systems will be examined later.

IIIB. Skeletal optical region; C–C stretching (1050–1150 cm^{-1})

The skeletal optical modes are highly sensitive to hydrocarbon state [6,15–18]. For long-chain hydrocarbons, of the three bands comprising this region, the two at 1064 and

1133 cm^{-1} are characteristic of all *trans* chain segments, while the third, at ≈1090 cm^{-1}, arises from chains containing *gauche* configurations and, in phospholipids, is superimposed upon the symmetric O-P-O stretching band. The skeletal-optical region can therefore be used to assess lipid chain configuration in systems composed predominantly of lipid. (The region is not readily analyzed in the presence of substantial amounts of protein, because of the diffuse C–C stretching contribution of these macromolecules.) Order ⇌ disorder transitions, e.g. of phospholipid acyl chains, are characterized by a drastic spectral alteration: the central *gauche* band broadens and shifts to lower frequency, the 1133 cm^{-1} *trans* band reduces in intensity and the 1064 cm^{-1} *trans* band, usually the sharpest and most intense C–C stretching feature of the ordered state, becomes a shoulder on the broadened *gauche* band. Because of these spectral changes various investigators have employed the $[I_{\approx 1064}/I_{\approx 1090}]$ or $[I_{\approx 1133}/I_{\approx 1090}]$ intensity ratios to monitor acyl chain order ⇌ disorder transitions. (In applying these ratios to phospholipid crystal ⇌ liquid-crystal transitions, it is assumed that the position and intensity of the O-P-O band remain unchanged throughout the transition.) For example, Yellin and Levin [17] have measured $[I_{1088}/I_{\approx 1133}]$ of hydrated dipalmitoyl phosphatidylcholine multilayers as a function of temperature to determine the cluster size of a cooperative unit undergoing a chain melting transition. The enthalpy, ΔH, was related to the Raman peak intensities by the integrated Van 't Hoff equation, i.e. in $[I_{1088}/I_{\approx 1130}] = \Delta H/RT + C$. An estimate of 31 molecules per cooperative cluster is presented.

Gaber and Peticolas [15] have recently refined the use of *trans-gauche* intensity ratios for the assessment of phospholipid crystal ⇌ liquid-crystal transitions. In this they assume that the intensity of the 1133 cm^{-1} band is the sum of the intensities from individual all-*trans* segments, independent of end group of neighbor effects. Then they measured scattering intensity, I, at 1133 cm^{-1} given by

$$I = I_0 \sum_{n=3}^{N} nC_n P_t^n$$

where I_0 is the intensity per '*trans*-unit', n is the number of bonds in an all-*trans* sequence within a chain of N bonds and C_n is the number of times the N-th segment recurs.

Gaber and Peticolas [15] then proceed to define a *trans* 'order parameter', S_{trans}, which, in analogy to the S_{lat} parameter already discussed is normalized so that $S = 1$ at highest possible order and $S = 0$ at no order (not necessarily minimal order). They define the *trans*-parameter for phospholipids in general as

$$S_{trans} = \frac{[I_{1133}/I_{ref}] \text{ observed}}{[I_{1133}/I_{ref}] \text{ phospholipid-solid}}$$

For very precise work on phosphatidylcholines, they suggest the use of I_{722} (I_{ref}); choline CN-stretching instead of I_{1090}.

Recently, Karvaly and Loshchilova [44] have questioned the applicability of the equations used to calculate S_{trans} [15]. These authors found that $S_{trans}{}^1$ and $S_{trans}{}^2$ values exceed the maximum theoretical value of unity when the dipalmitoyl phosphatidylcholine is hydrated in the presence of certain mono- and divalent cations. The reason for this could be that the reference bands, i.e. 772 cm^{-1} ($S_{trans}{}^1$) and 1096 cm^{-1} ($S_{trans}{}^2$), are not constant as assumed. These bands involve vibrations due to $C-N^+$ and PO_2^-, respectively. Cations, such as Ca^{2+} and Mg^{2+}, may have ordering effects through the

involvement of polar head groups and may influence the intensity of the reference bands. These studies suggest that some adjustment should be made in I_{ref} (crystalline).

IIIC. Acoustical and lattice vibrations (<400 cm^{-1})

IIIC (1). General considerations

Basic considerations [37,45–53] indicate that very important information on the order and state of membrane components should be obtainable by analysing the region below 400 cm^{-1}. The low frequency modes expected in this region would derive from (a) longitudinal acoustic vibrations of extended chains (representing accordion-like motions), and (b) lattice modes of lipid, protein and water [45] lattices. Such low frequency motions are collective, involving coherent movement of either long molecular chains or crystalline arrays. As such, their positions and intensities should be extremely sensitive to chain conformation, head group lattice structure, chain order and lipid phase.

Raman and infrared spectra of simple systems support the contention that such modes should be detectable in membranes. Thus, Brown et al. [50] detect a Raman mode in α-chymotrypsin, centered at $\approx$29 cm^{-1} and sensitive to the conformation of the protein. Furthermore, Genzel et al. [37] demonstrate, for crystalline egg white lysozyme, a 25 cm^{-1} band arising from intermolecular vibrations, related to lattice packing, a 75 cm^{-1} band due to torsion of α-helices and a 160 cm^{-1} band due to bending in β-structural chains. In addition, theoretical [51] and experimental [52] work on triclinic *n*-paraffins has been successful in assigning the low frequency bands of polymethylene solids and correlating the frequencies of these bands with the length of all-*trans* segments involved. Other data [53] show that a chain (helix) with a length approximately equal to the thickness of a biomembrane has a low frequency Raman mode at about 35 cm^{-1}.

Raman data on various liquid crystals reveal the existence of lattice modes, below about 150 cm^{-1} and sensitive to the phase of the sample [48–54]. Solid diethylazoxybenzoate shows a lattice mode at 22 cm^{-1} whose intensity decreases by 70% and whose frequency shifts to 14 cm^{-1} upon thermally-induced transition to the smectic A phase [54]. The band vanishes completely in the isotropic liquid. While we cannot now accurately estimate the frequencies of the corresponding modes of the liquid-crystalline or solid phospholipid arrays, it is certain that they will occur in the low frequency region, owing to the large masses of the molecules involved and the weakness of the bonding forces. The scarcity of current data on membrane head group structure, conformation and interactions and the probable sensitivity of lattice modes to these aspects of membrane physics makes the detection and assignment of these features of the Raman spectrum of membranes a particularly promising research goal.

IIIC (2). Phosphatidylcholine liposomes

We [27] have carried out a study on the acoustical-region bands of egg phosphatidylcholine and egg phosphatidylcholine/cholesterol (1 : 1; mol/mol liposomes above and below the transition temperature ($\approx$–5°C) of the phospholipid: upon changing the temperature from +18 to –11°C, a peak near 365 cm^{-1}, a shoulder near 350 cm^{-1} and a band at 290 cm^{-1} (presumably due to phosphate deformations) convert into sharp bands at 370, 350, and 310 cm^{-1}, respectively (Fig. 4). In addition, the asymmetrical band peaking at 260 cm^{-1} (not seen in chloroform solutions of phosphatidylcholine) persists to approx. –5.5°C, the transition temperature (T_c) of egg phosphatidylcholine but at lower temperatures shifts into a shoulder on a strong band at 245 cm^{-1}. The band at

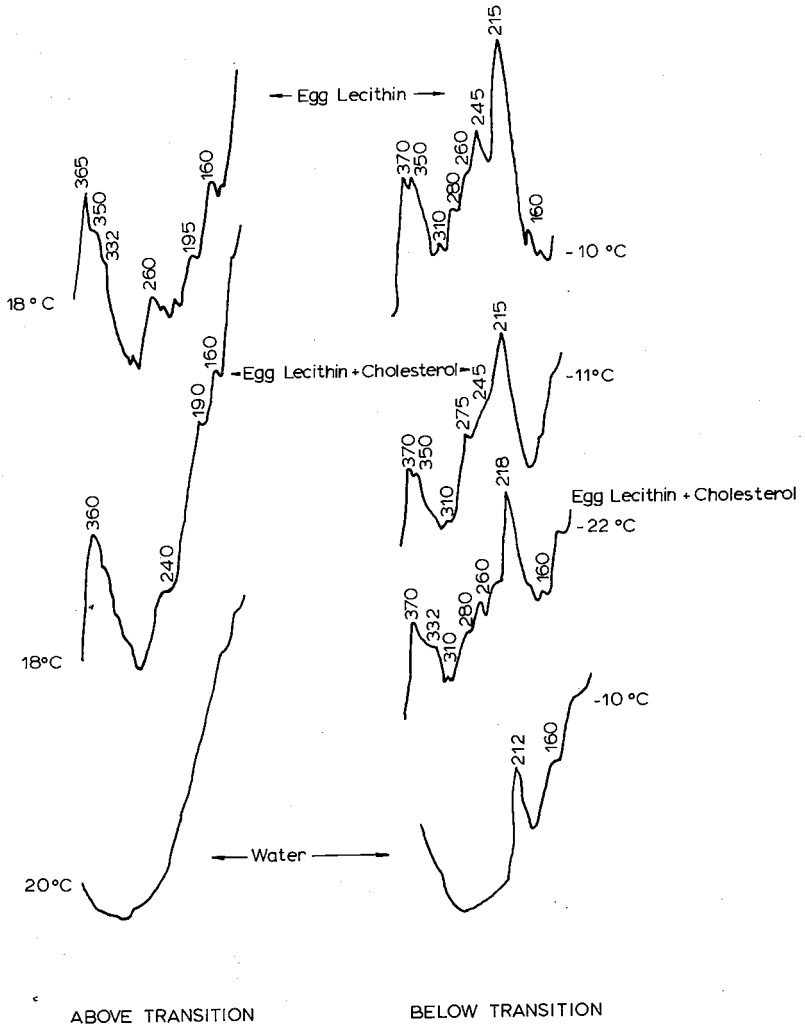

Fig. 4. Raman spectra in the acoustical region of egg phosphatidylcholine, egg phosphatidylcholine/cholesterol liposomes, and water above and below the egg phosphatidylcholine transition temperature. From Ref. 27.

195 cm^{-1} (also not seen in chloroform solution) disappears below the transition temperature. We cannot now provide assignment for these bands. The shoulder at 150–170 cm^{-1}, seen at all temperatures above freezing and whose frequency position varies inversely with temperature between −5 and 95°C is ascribed to hindered translation (ν_t) in liquid water. It coincides in position with the band expected from ordered palmitate chains, but at 18°C (above T_c) such chains in egg phosphatidylcholine should not be ordered. Upon freezing, which here occurs between −1 and −2°C due to supercooling, the strong ν_t band of ice I appears at 215 cm^{-1}. As expected, this band shifts to higher frequencies with decreasing temperature. It lies at 218 cm^{-1} at −30°C and probably corresponds to the 218 cm^{-1} band, previously attributed to crystalline oleate in aqueous sonicates of dioleoyl phosphatidylcholine at −62°C [55]. The strong band which appears at $>T_c$ is

attributed to ordered oleate chains in the phosphatidylcholine.

The deformity, below T_c of the low frequency limb of the 210 cm^{-1} ice I band (Fig. 4) can be shown by derivative spectroscopy to arise from a band at 208 cm^{-1}, due to ordered oleate chains in the phosphatidylcholine. The feature, below T_c at $\approx$160 cm^{-1} is attributed to ordered palmitate and oleate chains (and possibly residual, unfrozen water).

IIIC (3). Sphingomyelin and phosphatidylethanolamine

Mendelsohn et al. [13] find that solid lauric acid at −160°C (crystalline) gives a lauric acid acoustical mode at 205 cm^{-1}, as well as bands at 119 and 171 cm^{-1}, thought to be torsional or lattice modes. Above the melting temperature only a broad, weak feature at 234 cm^{-1} remains. This is thought to reflect a decrease in the average all-*trans* chain length, i.e. the length of the coupled segments.

In contrast, dilauroyl phosphatidylethanolamine at −165°C, yields broader, weaker features at 224 and 138 cm^{-1} with shoulders at 218 and 148 cm^{-1}. All of these components disappear almost fully with melting. The authors suggest that the 218–224 cm^{-1} feature of the phospholipid corresponds to the 205 cm^{-1} acoustical mode of lauric acid and that the differences between the two situations relate to chain packing.

IV. Raman spectra of mono- and multilamellar phospholipid dispersions in water

When solid phospholipids are hydrated and coarsely dispersed, they form large liposomes consisting of concentric multilamellar bilayer shells. However, a number of techniques, particularly sonication ± gel permeation chromatography, allow one to isolate instead a population of unilamellar vesicles of 250–300 Å diameter.

Mendelsohn et al. [14] have compared two such types of liposome prepared from egg and dipalmitoyl phosphatidylcholine above and below the crystal ⇌ liquid-crystal transition temperature. They found no change upon sonication, in the *trans/gauche* ratio of dipalmitoyl phosphatidylcholine above and below the transition temperature and no reliable change for egg phosphatidylcholine. In contrast, some decrease in $[I_{\approx 2890}/I_{\approx 2850}]$ was observed following sonication. This was interpreted as possibly indicating less complete chain packing in small vesicles, due to the decreased radius of curvature.

A similar study was carried out by Spiker and Levin [11], for dipalmitoyl and dimyristoyl phosphatidylcholine above and below the phase transition. To follow intensities accurately, internal standards were employed. The authors found a broadening of the crystal ⇌ liquid crystal transition. They suggest, on the basis of $[I_{1129}/I_{1097}]$ and $[I_{1064}/I_{1097}]$ ratios, that vesicles contain a greater proportion of *gauche* conformers. In addition comparisons of $[I_{2882}/I_{2847}]$ for the phospholipids in polycrystalline, multibilayer and vesicle states indicate lesser interaction between chains in the monolamellar vesicles.

Gaber and Peticolas [15] have readdressed this matter recently. They conclude, on the basis of comparisons of S_{lat} for multi- and unilamellar liposomes, that interchain packing is significantly reduced in the latter. They also find that the chain melting curves for vesicles determined by CH-stretching measurements always lie at lower temperatures than curves derived from C–C stretching. This is not true for multilamellar systems. They conclude that the same *trans/gauche* proportions exist in multi- and unilamellar systems, but that their interconversion is restricted in the former.

Recently, Gaber et al. [56] used Raman difference spectroscopy [57] to analyze aqueous dispersions of dipalmitoyl phosphatidylcholine in the following temperature

regions: below the pretransition ($34 \pm 2°C$), between the pretransition and the order $\rightleftharpoons$ disorder transition ($42°C$) and above the order $\rightleftharpoons$ disorder transition. The difference spectra, produced by computer subtraction of absolute spectra in the regions of CH-stretching, CH-deformation, as well as C—C-stretching, indicate a distinct lipid conformation in each of the three temperature ranges defined. Below the pretransition temperatures the decrease in intensity of bands at 1062, 1100, and 1129 cm^{-1} in the difference spectra (absolute spectra at $15°C$ minus spectra at $36°C$) suggest a loss in the number of *trans* bonds. The absence of the *gauche* band at 1080 cm^{-1} further indicates that *gauche* bonds occur singly between long *trans* segments or in the terminal segments of acyl chains. The authors calculated an order parameter (S_{trans}) which decreases from 0.85 to 0.75 upon heating the bilayer from 15 to $32°C$. This change corresponds to an increase of about one *gauche* bond per chain [15]. The appearance of a band at 2860 cm^{-1}, previously assigned to symmetric CH_2-stretching in the triclinic crystalline structure of fatty acids [58], and a change in intensity at 2845 and 2881 cm^{-1}, further suggests that phospholipids below their pretransition temperatures may be in a triclinic array.

Between the pretransition and main transition, the lipids are in loose hexagonal phase. Upon melting ($37–50°C$ difference spectrum) the 1062 and 1128 cm^{-1} bands decrease further in intensity. The 1080 cm^{-1} band gains intensity above the melting transition, indicating appearance of sequences of closely coupled *gauche* bonds and reduction in *trans* segments.

The CH_2-scissoring and CH_2-stretching change in intensity at pretransition temperatures. There is an intensity loss of 1435 and 1460 cm^{-1}, and a gain at 1444 cm^{-1}. In the CH-stretching region, the intensity at 2882 cm^{-1} decreases almost twice as much as at 2843 cm^{-1}. This suggests that, lateral interactions in the pretransition range decrease.

Upon going above the main transition temperature of dipalmitoyl phosphatidylcholine, the 1080 cm^{-1} band becomes broad and strong, a large intensity decrease occurs at 2880 cm^{-1} and the 2943 and 2880 cm^{-1} bands shift to 2853 and 2890 cm^{-1}, respectively. The main transition therefore involves a loss of chain-chain interaction and a sharp increase in the number of *gauche* bonds.

V. Cholesterol-phospholipid systems

VA. Introduction

Faiman [59] has recently reported a detailed Raman spectroscopic study of different forms of cholesterol and its derivatives in the crystalline state. However, because of the important effect of cholesterol on membrane structure and function more work has been done on cholesterol phospholipid systems. In this context, Hinz and Sturtevant [60] have shown that the transition width for the dimyristoyl phosphatidylcholine-cholesterol system is a nearly linear function of the cholesterol mol fraction between 0 and 0.2. Very likely cholesterol clustering occurs at higher mol fractions, such as occur in plasma membranes. Such clustering is suggested by probe studies.

VB. CH-stretching region

Verma and Wallach [27], following the [I_{2885}/I_{2850}] CH-stretching ratio, found a drastic broadening also of the crystal $\rightleftharpoons$ liquid crystal transition of egg phosphatidylcholine, at a cholesterol/phospholipid molar ratio of 1.0 (Fig. 5). Importantly, Bunow

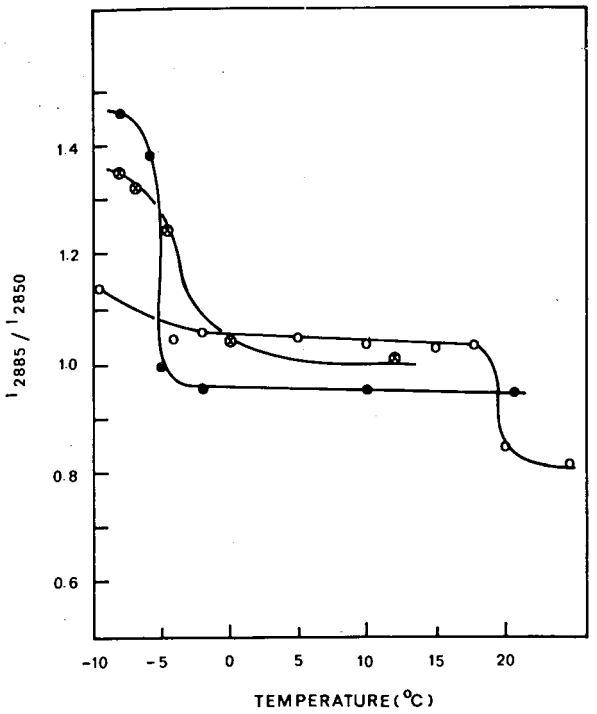

Fig. 5. Variation of $[I_{2885}/I_{2850}]$ with temperature for liposomes composed of egg phosphatidylcholine (•), egg phosphatidylcholine/cholesterol (1 : 1, mol/mol) (⊗), and egg phosphatidylcholine/melittin (25 : 1, mol/mol) (○). Values represented are averages of 3 recordings on 3 different preparations (range 15%). From Ref. 20.

and Levin [33] noted that the crystal ⇌ liquid crystal transition of 3 : 1 (mol/mol) dimyristoyl phosphatidylcholine/cholesterol was 16°C broader, according to the $[I_{2880}/I_{2850}]$ ratio, than that of the sterol free lipid.

VC. Skeletal-optical region

Lippert and Peticolas [6], following $[I_{1089}/I_{1128}]$ for dipalmitoyl phosphatidylcholine and dipalmitoyl phosphatidylcholine-cholesterol (1 : 1, mol/mol) showed that cholesterol changed transition of the phospholipid from a 'cooperative event', occurring over <2°C to a poorly cooperative one, extending over more than 40°C. The data also suggest a suppression of *gauche* isomerization above the transition temperature and a reduction of all *trans* conformers below the transition. This supports other data indicating that cholesterol acts as a 'buffer' for chain fluidity.

In a related study, Mendelsohn [8], using an egg phosphatidylcholine-cholesterol (1 : 1, mol/mol) system and monitoring the skeletal optical region, came to the conclusion that, above the phospholipid transition temperature the sterol inhibited the formation of *gauche* isomers, tending to make the acyl chains more rigid. Concordant results were obtained by Spiker and Levin [11] who found a transition broadening of approx. 24°C for cholesterol-dipalmitoyl phosphatidylcholine (1 : 3, mol/mol) multilayers. These workers also noted an increase in the proportion of *gauche* conformers

below the transition temperature of multilayers but no effect on the proportion of *gauche* conformers in vesicles.

VD. Egg phosphatidylcholine-cholesterol liposomes; acoustical region

As shown in Fig. 4, egg phosphatidylcholine-cholesterol liposomes (1 : 1, mol/mol) exhibit different low-frequency spectra from sterol-free liposomes both above and below −5.5°C the phosphatidylcholine transition temperature [27]. The 260 cm^{-1} band of phosphatidylcholine liposomes above T_c is replaced by a weak shoulder at approx. 240 cm^{-1}. At −11°C the phosphatidylcholine-cholesterol spectrum differs from the corresponding phosphatidylcholine spectrum in that the prominent 245 cm^{-1} band (attributed to oleate) is reduced to a broad shoulder. The 245 cm^{-1} band does not resolve even at −22°C, although the 260 cm^{-1} band does emerge at that temperature (Fig. 4).

The results suggest that above the transition temperature, the presence of cholesterol perturbs the lattice structure of phosphatidylcholine head groups. Below the phosphatidylcholine transition temperature the sterol impedes the ordering of acyl chains (cf. lacking 245 cm^{-1} band). This is what is expected from the established behavior of cholesterol.

VI. Raman active probes

VIA. Phospholipid systems containing conjugated polyenes

We have [24], in our initial Raman study of hemoglobin free erythrocyte ghosts, observed two prominent bands at 1530 and 1165 cm^{-1} which we proved to represent ν(–C=C–) and ν(=C–C=), respectively, of membrane-associated β-carotene [12,24]. The length of the β-carotene polyene chain is such that it can only be accommodated by a phospholipid bilayer if its orientation is other than normal to the membrane plane. The resonance-enhanced bands in both erythrocyte ghosts and phosphatidylcholine or egg phosphatidylcholine-cholesterol liposomes were then studied, using the 1440 cm^{-1} HCH deformation band as a reference. It was found that the ratio $[I_{1527}/I_{1440}]$ decreased precipitously with cholesterol/phospholipid ratio, reaching a minimum value at a cholesterol/phospholipid ratio near 0.9. However, the relative intensities of the 1527 and 1158 cm^{-1} resonance-enhanced bands remained constant throughout. The results suggest that β-carotene is not simply accommodated in phosphatidylcholine liposomes containing cholesterol and almost not at all so at a cholesterol/phospholipid molar ratio near 1. The changes in the resonance-enhanced bands were attributed to extrusion of the β-carotene chain from cholesterol-containing regions.

Bunow and Levin [33] have examined the resonance-enhanced and normal Raman spectra of amphotericin B associated with multilamellar and unilamellar vesicles of dimyristoyl phosphatidylcholine ± cholesterol. Amphotericin B is a conjugated polyene antibiotic which has a high affinity for cholesterol ($K_c = 2.6 \cdot 10^6$ M^{-1}). In combination with cholesterol in many systems, but not the plasma membranes of simian virus 40 transformed cells [61–62], amphotericin B forms transmembrane hydrophilic channels.

Bunow and Levin [33] followed the intensity of the amphotericin B ν(–C=C–) band (1556 cm^{-1}) under various conditions and observed that its relation to other resonance-enhanced polyene bands was constant, and that the antibiotic did not interact with

apolar phospholipid chains of dimyristoyl phosphatidylcholine in the absence of cholesterol. However, in phosphatidylcholine-cholesterol systems (4 : 1, mol/mol) the intensity of the 1556 cm^{-1} band monitored the cholesterol-broadened crystal ⇌ liquid crystal transition of the lipid system.

Bunow and Levin [33] also monitored the effect of amphotericin B on phospholipid chain structure, by measuring $[I_{2880}/I_{2850}]$ and $[I_{2935}/I_{2850}]$. Their data indicate that the cholesterol-induced broadening by cholesterol (cholesterol/phospholipid, 1 : 4, mol/mol) from <1°C for dimyristoyl phosphatidylcholine to 16–32°C, is reduced by amphotericin B, suggesting a cholesterol/antibiotic stoichiometry of 1 : 1 (24°C), supported by calorimetric data. For cholesterol-containing systems $[I_{2935}/I_{2850}]$ increased in the presence of the antibiotic suggesting its penetration to the methyl region of the bilayer. However, $[I_{2880}/I_{2850}]$ was increased even in the absence of cholesterol, implying a sterol-independent ordering of phospholipid acyl chains.

Overall, the results for cholesterol/phospholipid (1 : 4, mol/mol) systems indicate that amphotericin B is ordered in lipid-cholesterol media as in a solid, but that its environment is a little more polar. In addition bulk acyl chain transitions clearly modulate the structure of amphotericin B-cholesterol-phosphatidylcholine complexes.

Concerning the behavior of conjugated polyenes in biomembranes, information at the present is restricted to our earlier work [24] on erythrocyte ghosts. In the screening studies, we found that several membrane perturbations, trypsinization, lysophosphatidylcholine, and reduction of pH, increased the relative intensity of the resonance-enhanced β-carotene bands, whereas heating (50°C; 15 min) or addition of 0.1% sodium dodecyl sulfate decreased their intensity. We proposed that membrane-associated β-carotene is not a fully extended or fully folded configuration. Since carotenoid electronic spectra are sensitive to such factors, membrane structure changes leading either to free extension of β-carotene chains, or the folding of these chains, would appear in the resonance Raman spectra. We accordingly suggested the use of conjugated polyenes as 'Raman-active' probes of biomembrane structure.

VIB. Deuterated probes

The methyl and methylene contributions of both lipids and proteins in the CH-stretching region generally overlap and in biomembranes or in lipid-protein mixtures it may become difficult to distinguish between changes occurring in lipids or in proteins. Mendelsohn et al. [13,63] have attempted to circumvent this problem by using deuterated fatty acids and deuterated phospholipids.

The C^2H-stretching bands occur in the 2100 cm^{-1} region and signals of specifically deuterated acyl chains are free from interfering bands. In spite of this advantage there are reservations about using free deuterated fatty acids as a probe for the following reasons. The intensity of C^2H-stretching vibrations is comparable to those of CH-stretching vibrations. One therefore needs a minimum concentration of 5–10 mg/ml to record a good spectrum. This concentration is about 50% of the weight generally used for the preparation of phospholipid liposomes for Raman spectroscopy, and fatty acids at such concentrations perturb the thermal transition of phospholipids (Ref. 64; Wallach, D.F.H. and Verma, S.P., unpublished results).

On the other hand deuterated fatty acids and deuterated phospholipids can be suitably used to investigate their own behavior in mixed lipid systems and in lipid-protein recombinants. Thus Mendelsohn and Maisano [63] studied thermal transition by following

the C^2H-stretching vibrations (2100 cm^{-1} region) of the deuterated-d_{58} derivative of dimyristoyl phosphatidylcholine mixed with distearoyl phosphatidylcholine (1 : 1, mol/mol). The line width of the 2103 cm^{-1} feature (C^2H-stretching vibration) was sensitive to temperature and exhibited inflections at the crystal ⇌ liquid-crystal phase transitions. These studies clearly revealed two distinct transitions at 28 and 47°C, respectively. Deuterated probes are useful, therefore, when the deuterated molecules themselves are the components under investigation. They cannot be used in the manner of ESR or fluorescence probes.

VII. Phospholipid-iodine-iodide system

The presence of iodine species (I_2, I^-, I_3^- and other polyiodide ions) drastically increases the electrical conductivity of black lipid membranes. The change in electrical conductivity has been explained on the basis of ionic conduction [65,66] and electronic conduction with donor-acceptor complex formation [67]. Loshchilova and Karvaly [68] used Raman spectroscopy to study iodine-lipid interactions. They compared the intensity ratios $[I_{1092}/I_{1066}]$, $[I_{1092}/I_{1128}]$ and $[I_{2850}/I_{2882}]$ in dipalmitoyl phosphatidylcholine dispersions containing iodine species (I_2, I^-, I_3^-). In controls these ratios are 0.51, 0.67 and 0.80, respectively. The presence of I_2 increases the ratios to 0.67, 0.85, 0.86, respectively, indicating a disordering effect due to the formation of iodine-lipid complexes. However, more drastic effects are noticed in the presence of higher concentrations of KI where the ratios increase to 1.04, 1.94 and 1.12, respectively. The authors suggest that, upon exposure to a laser beam, I_2 and polyiodide ions may generate as a result of oxidation and that these may penetrate into the lipid phase. In order to eliminate the possibility of direct interactions of I^- and I_3^- with hydrocarbon chains, $2 \cdot 10^{-2}$ M K_2SO_5 was used as an oxidizing agent and alternative source of perturbation. Under such conditions, the ratios remained almost unchanged. The authors therefore suggest that I_2 (not complex iodide species) is the primary source for the resistance-lowering effect in black lipid membranes [65–67].

VIII. Polypeptide-phospholipid systems

VIIIA. Melittin

Verma and Wallach [20] have evaluated the thermal behavior of liposomes made of egg phosphatidylcholine or dimyristoyl phosphatidylcholine, as well as of liposomes composed of phosphatidylcholine plus cholesterol, phosphatidylcholine plus β-carotene and phosphatidylcholine plus melittin. Melittin is a membrane active polypeptide from bee venom in which the apolar residues lie at one end of the polypeptide chains. The first 20 residues from the NH_2-terminal comprise principally apolar entities, while the COO^- terminus consists of the basic sequence -Lys-Arg-Lys-Arg-Glu-Gln. This substance appears to intercalate its apolar residues among the relatively liquid fatty acid chains of a phosphatide bilayer in a random array. To monitor lipid chain thermal responses, the variation with temperature of Raman scattering due to CH-stretching vibrations and of resonance-enhanced Raman scattering due to the –C=C– and =C–C= stretching vibrations of membrane-bound β-carotene were followed in liposomes composed of phosphatidylcholine (egg, dimyristoyl, or dipalmitoyl) ± cholesterol, β-carotene or melittin in the temperature range of –10 to 45°C.

Plots vs. temperature of the intensities of the ≈2885 and ≈2930 cm^{-1} CH-stretching bands relative to the intensity of the thermally stable 2850 cm^{-1} band, i.e. the $[I_{2885}/I_{2850}]$ and $[I_{2930}/I_{2850}]$ ratios, revealed a sharp discontinuity in cholesterol-free phosphatidylcholine liposomes (Fig. 5). This coincides with the gel ⇌ liquid-crystal transition temperature of the fatty acyl chains. In cholesterol-phosphatidylcholine liposomes the change in $[I_{2885}/I_{2850}]$ occurred over a broad temperature range and $[I_{2930}/I_{2850}]$ remained stable (Fig. 5). $[I_{1527}/I_{1158}]$, i.e. the intensity of ν(–C=C–) relative to that of ν(=C–C=) in β-carotene-phosphatidylcholine liposomes, changed discontinuously with the gel ⇌ liquid-crystal transition. The values above the transition temperature approached those of the carotenoid in organic solution.

The transitions reported in $[I_{2930}/I_{2850}]$ for egg phosphatidylcholine-melittin liposomes (25–56 : 1, mol/mol) were shifted to much higher temperatures than observed in egg phosphatidylcholine liposomes [20]. In the case of dimyristoyl phosphatidylcholine-melittin the change in $[I_{2930}/I_{2850}]$ also occurred at a higher temperature (28°C) than without melittin (21°C) (Fig. 6), but the temperature shift was less than the 13°C observed for $[I_{2885}/I_{2850}]$. It appears that the apolar moiety of melittin organizes phospholipids adjacent to and more remote from the peptide moiety, to form complexes with and elevate the lipid transition temperature. The effect of the peptide moiety may be greater on the methylene segments because of the greater response of $[I_{2885}/I_{2850}]$

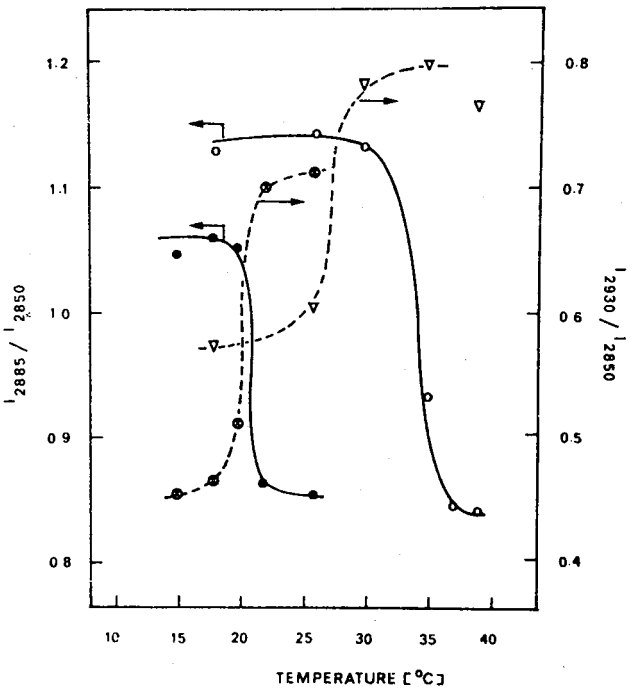

Fig. 6. Variation of temperature of $[I_{2885}/I_{2850}]$ and $[I_{2930}/I_{2850}]$ of liposomes composed of dimyristoyl phosphatidylcholine/melittin. •, dimyristoyl phosphatidylcholine $[I_{2885}/I_{2850}]$; ○, dimyristoyl phosphatidylcholine/melittin (28 : 1, mol/mol), $[I_{2885}/I_{2850}]$; ⊗, dimyristoyl phosphatidylcholine $[I_{2930}/I_{2850}]$; ▽, dimyristoyl phosphatidylcholine/melittin (28 : 1, mol/mol), $[I_{2930}/I_{2850}]$. The numerical values marked for the ratios are averages calculated from 3 different recordings on 3 different samples (range ±7%). From Ref. 20.

than $[I_{2930}/I_{2850}]$. Control studies (unpublished) indicate that the observed effects were not due to melittin-associated Raman scattering in the regions examined.

An important finding in this study is that the interaction of melittin with phospholipids produces a drastic rise in the transition temperature of the phospholipid acyl chains. Moreover, the effect occurs at low molar ratios of melittin to phospholipid. This indicates that the polypeptide affects at least the phospholipid immediately adjacent to it and probably also imposes constraints extending over several layers of lipid surrounding the polypeptide. In the case of dimyristoyl phosphatidylcholine, there may also be a gradient of structuring perpendicular to the membrane plane, with a greater effect on methylenes $[I_{2885}/I_{2850}]$ than on methyl termini $[I_{2930}/I_{2850}]$. In any event the results suggest that melittin can impose a long-range organization of phospholipid chains through apolar interactions.

VIIIB. Valinomycin, alamecithin

Several investigators have studied the effects of peptide ionophores on the lipid chain structure of phospholipid bilayers. Thus, Lis et al. [19] have examined the action of valinomycin, a K^+ carrier, and alamecithin, thought to act as a polar transmembrane pore. Comparing the $[I_{1064}/I_{1089}]$ ratios of dipalmitoyl phosphatidylcholine liposomes in the crystal state and dimyristoyl phosphatidylcholine liposomes supposedly in the liquid-crystal state with and without valinomycin or alamecithin, they found the following: (a) no change in the *trans/gauche* proportion of dipalmitoyl phosphatidylcholine at any concentration of valinomycin or alamecithin, and (b) an increase in the proportion of *gauche* conformers in the case of both peptide complexes with dimyristoyl phosphatidylcholine. The significance of these findings is not clear, since the presented spectrum of dimyristoyl phosphatidylcholine suggests that the phospholipid was in the crystalline state, not liquid-crystalline as suggested. The preferential interaction of valinomycin and alamecithin with dimyristoyl phosphatidylcholine might thus be attributed to lesser interchain stabilities than in the case of dipalmitoyl phosphatidylcholine.

VIIIC. Gramicidin

In a more recent study, Weidekamm et al. [69] examined the interaction of gramicidin A with dipalmitoyl phosphatidylcholine and dipalmitoyl phosphatidylcholine-cholesterol liposomes. (Gramicidin A is a pentadecapeptide ($M_r = 1700$) which forms transmembrane ion-permeable channels, probably as a helical dimer.) They followed the $[I_{2883}/I_{2847}]$ ratio to monitor methylene CH-stretching, the $[I_{2936}/I_{2847}]$ ratio to monitor methyl CH-stretching and $[I_{1089}/I_{1128}]$ to monitor *trans/gauche* proportions, all between 20 and 60°C.

At a gramicidin A/dipalmitoyl phosphatidylcholine molar ratio of 1 : 650 the thermotropic transition (at 40°C) of phospholipid methylene groups was broadened but that of the methyl groups was unaffected. At a molar ratio of 1 : 150 the methylene transition was eliminated and that of the methyl residues shifted upward by 2–3°C. Measurements of $[I_{1089}/I_{1128}]$ vs. temperature revealed a broadening (but no shift) of the chain transition at 40°C.

Interestingly, the gramicidin effects on the CH-stretching ratios became reduced by incorporation of cholesterol into the liposomes. Dipalmitoyl phosphatidylcholine/cholesterol liposomes even in the presence of high proportions of gramicidin A show the

poorly cooperative thermotropic phase transitions typical of phosphatidylcholine-cholesterol systems.

The results of Weidekamm et al. [69] clearly demonstrate a profound perturbation of lateral interactions between phospholipid acyl chains by the polypeptide, a perturbation anticipated from the theoretical considerations already presented. The data also indicate that this perturbation is not uniform at varying depths of the bilayer.

In many ways the action of gramicidin A is similar to that of cholesterol. This sterol interferes with interactions between phospholipid hydrocarbon chains, thereby reducing the cooperativity of thermotropic phase transitions. However the cholesterol effects occur only at cholesterol-phospholipid molar ratios greater than 0.2, whereas the gramicidin A effects are very evident already at a molar ratio polypeptide/phospholipid of about 0.0015. This suggests a long-range effect imposed on the phospholipid acyl chains through interaction of the apolar amino acid side chains with the phospholipid hydrocarbon residues, an effect possibly similar to that described above for melittin and below for proteolipid apoproteins.

IX. Phosphatidylcholine-protein system

IXA. Phosphatidylcholine-proteolipid apoprotein 'recombinants'

IXA (1). Introduction

An important role has been discovered for proteolipids in membrane transport [70, 71]. As reviewed in Ref. 71, proteolipids, operationally defined as protein-lipid complexes soluble in chloroform/methanol mixtures, were first isolated from bovine white matter tissue; however, they also occur in a wide variety of non-neural tissues and appear quite concentrated in mitochondria. A 12 000 dalton proteolipid is also present in sarcoplasmic reticulum Ca^{2+}-ATPase and, together with phospholipids, is required to form Ca^{2+}-transport vesicles [70,72,73]. A role of proteolipids in the formation of functional, vesicular sodium pump vesicles has also been suggested [73,74] and Racker [71,72] proposes that proteolipids act as or bear cation ionophores.

Proteolipid apoprotein is the delipidated form of the white matter proteolipid and is the most abundant protein of myelin sheath membranes. The amino acid composition of proteolipid apoprotein (more than 50% apolar residues), its solubility in chloroform/methanol, and the presence of 2–3% covalently bound fatty acids in its structure suggest a role as an integral membrane protein in myelin [75]. Recent freeze-fracture electron microscopy studies [76] also suggest that this protein is deeply embedded in the myelin lipid apolar regions. Proteolipid apoprotein is highly α-helical in chloroform/methanol (2 : 1, v/v), a solvent in which the protein is monomeric and can be converted to a water-soluble form in which the protein is present as a large aggregate of low helical content. Proteolipid apoprotein can be reassociated with diverse lipids by cosolution in chloroform/methanol [75] or 2-chloroethanol [77] and subsequent replacement (by dialysis) of the organic solvent with aqueous buffers. We have used this recombination approach in a Raman spectroscopic analysis of the structural influence of this type of 'integral' membrane protein, upon defined membrane lipids [22].

IXA (2). CH-stretching

We have examined the CH-stretching and C–C-stretching regions of proteolipid apoprotein-phosphatidylcholine vesicles (1 : 20, w/w, or at a molar ratio of $\approx$1 : 700), as a

function of temperature, using dimyristoyl phosphatidylcholine and egg phosphatidylcholine, and have integrated the study with observations by differential scanning calorimetry and X-ray diffraction [78].

The CH-stretching Raman spectrum of dimyristoyl phosphatidylcholine in the 2800–3000 cm^{-1} region (Fig. 7) exhibits, as previously-described, bands arising from both fundamental CH-stretching vibrations and their interactions with HCH deformation overtones of the phospholipid acyl chains. Spectra of dimyristoyl phosphatidylcholine/proteolipid apoprotein recombinant (20 : 1, w/w; or 700 : 1, mol/mol) at temperatures below (20°C) and above (37°C) the phosphatidylcholine order ⇌ disorder transition (Fig. 7) appear qualitatively the same as spectra of dimyristoyl phosphatidylcholine alone, except that the ≈2880 cm^{-1} band does not shift to 2890 cm^{-1} immediately above 23°C, as in dimyristoyl phosphatidylcholine per se, but only at about 41°C or higher temperatures.

$[I_{2880}/I_{2850}]$ is plotted as a function of temperature for dimyristoyl phosphatidylcholine and a dimyristoyl phosphatidylcholine/proteolipid apoprotein (20 : 1, w/w) recombinant in Fig. 8. In the case of dimyristoyl phosphatidylcholine alone the ratio decreases from ≈1.2 to ≈0.85 at the dimyristoyl phosphatidylcholine transition temperature. The recombinant, in contrast, shows an initial sharp decrease of intensity ratio at 23°C, followed by a slower decline. Even at 40°C, the intensity ratio of the recombinant has not reached the minimum value (for vesicles) attained by dimyristoyl phosphatidylcholine above the crystal ⇌ liquid-crystal transition.

A comparison of the thermal behavior of egg phosphatidylcholine and egg phos-

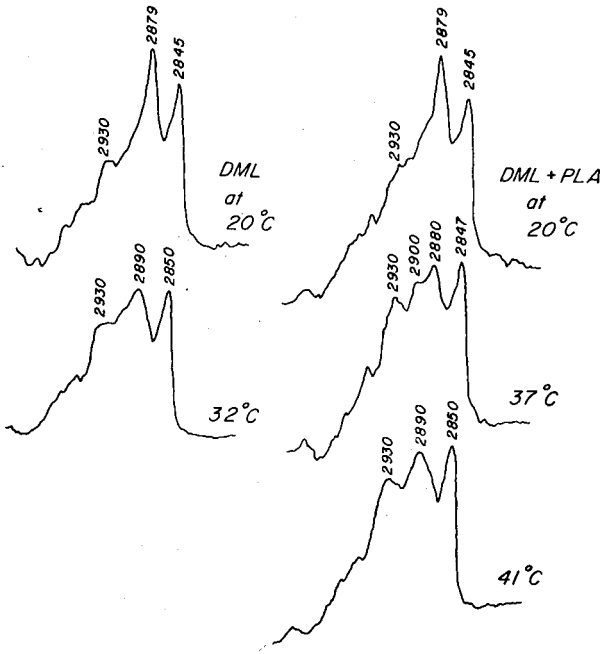

Fig. 7. Raman spectra of dimyristoyl phosphatidylcholine (left) and 20 : 1 (w/w) dimyristoyl phosphatidylcholine/proteolipid apoprotein (right) in the 2800–3000 cm^{-1} (CH-stretching) region. From Ref. 22, by courtesy of Biochemistry.

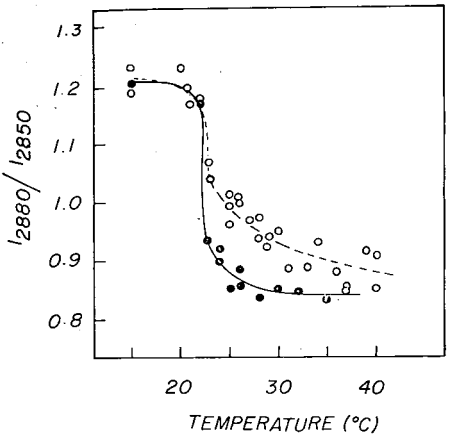

Fig. 8. [$I_{\approx 2880}/I_{\approx 2850}$] as a function of temperature for dimyristoyl phosphatidylcholine (———), and a 20 : 1 (w/w) dimyristoyl phosphatidylcholine/proteolipid apoprotein recombinant (- - - - - -). From Ref. 22, by courtesy of Biochemistry.

phatidylcholine-proteolipid apoprotein recombinants (20 : 1, w/w) in the CH-stretching region again shows striking differences (Fig. 9). In the presence of proteolipid apoprotein, the egg phosphatidylcholine transition becomes very broad, with undefined onset and completion temperatures. [$I_{\approx 2880}/I_{\approx 2850}$] for the recombinant is significantly greater than that for egg phosphatidylcholine alone at temperatures below that of the egg phosphatidyl transition, while above 15°C both egg phosphatidylcholine and the recombinant reach about the same minimum ratio. In addition, a new transition centered at about 12°C, appears; this is also detectable by differential thermal calorimetry.

IXA (3). Skeletal-optical region

The C–C-stretching region of phosphatidylcholine and recombinants (Fig. 10) was

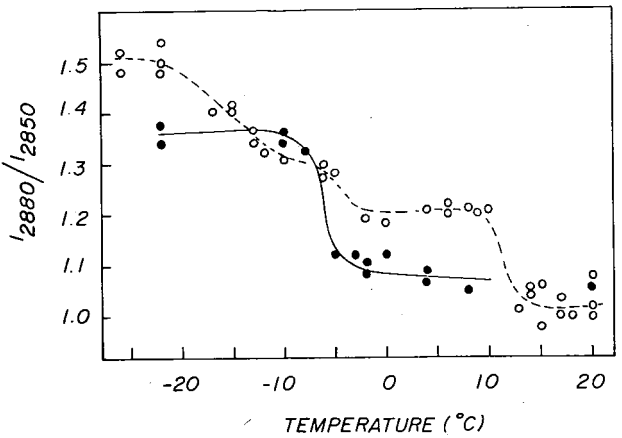

Fig. 9. [$I_{\approx 2890}/I_{\approx 2850}$] as a function of temperature for egg phosphatidylcholine (- - - - -) and a 20 : 1 (w/w) egg phosphatidylcholine/proteolipid apoprotein recombinant (———). From Ref. 22, by courtesy of Biochemistry.

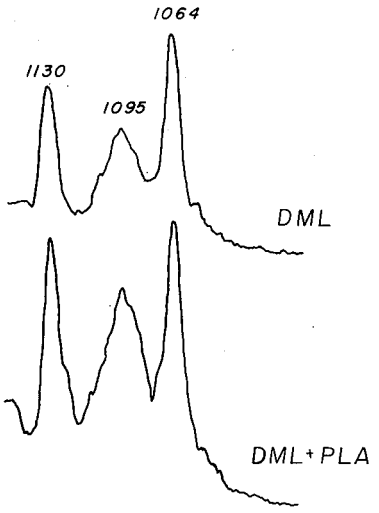

Fig. 10. Characteristic Raman spectra of dimyristoyl phosphatidylcholine and a 20 : 1 (w/w) dimyristoyl phosphatidylcholine/proteolipid apoprotein recombinant in the 1000–1150 cm^{-1} (C-C stretching) region at 20°C. From Ref. 22, by courtesy of Biochemistry.

analyzed using a modification of the S_{trans} order parameter of Gaber and Peticolas [15], specifically:

$$S_{\text{trans}} = \frac{[I_{1064}/I_{1095}]\ \text{sample} - [I_{1064}/I_{1095}]\ \text{liquid-crystalline phosphatidylcholine}}{[I_{1064}/I_{1095}]\ \text{gel phosphatidylcholine} - [I_{1064}/I_{1095}]\ \text{liquid-crystalline phosphatidylcholine}}$$

As already noted, this order-parameter varies between 0 and 1.0, where zero defines the acyl chain order of liquid-crystalline (melted chain) phosphatidylcholine but does not imply a truly random state. The maximum value, 1.0, defines the phosphatidylcholine acyl chains in the gel (rigid chain) state. Below the crystal ⇌ liquid-crystal transition of dimyristoyl phosphatidylcholine $[I_{1064}/I_{1095}]$ is maximally 2.45 and above the transition (at 35°C), 0.28. In the case of dimyristoyl phosphatidylcholine-proteolipid apoprotein (20 : 1, (w/w) the ratio is 1.80 below the transition and 0.48 even at 35°C, 12°C above the transition temperature.

The results thus indicate that at temperatures well below that of the crystal ⇌ liquid-crystal transition of dimyristoyl phosphatidylcholine the acyl chains of the complex ($S = 0.68$ at 20°C) possess more *gauche* conformation on the average than those of the phosphatidylcholine alone ($S = 0.98$ at 20°C). Thus some phosphatidylcholine acyl chains are prevented by proteolipid apoprotein from crystalling into their all-*trans* form below the phosphatidylcholine transition temperature. At 30°C, a temperature above that of the crystal ⇌ liquid-crystal transition, the order parameter for the recombinant ($S = 0.41$) is larger than that for dimyristoyl phosphatidylcholine alone ($S = 0.0$), indicating that the phospholipid acyl chains in the recombinant possess more *trans* configuration, on the average than would occur in pure liquid-crystalline dimyristoyl phosphatidylcholine. The phosphatidylcholine-proteolipid apoprotein complex thus contains a population of phospholipid molecules whose acyl chains have not converted into the fully liquid-crystalline state.

IXA (4). Interpretation

As noted earlier the CH-stretching region provides information about acyl chain interactions. That the dimyristoyl phosphatidylcholine-proteolipid apoprotein recombinant shows an initial sharp decrease in $[I_{2880}/I_{2850}]$ at approx. 22°C followed by a broader decline, suggests two phosphatidylcholine populations in the presence of proteolipid apoprotein: one whose acyl chain melting is relatively unperturbed by the protein, and another whose acyl chain thermal behavior is affected by its association with proteolipid apoprotein. Concordant results have been observed by Curatolo et al. [78] using differential scanning calorimetry. Also, the CH-stretching spectra of the recombinants with dimyristoyl phosphatidylcholine show a 2880 cm^{-1} feature at a 24–37°C, whereas dimyristoyl phosphatidylcholine alone only yields a 2890 cm^{-1} band. As already noted, the 2890 cm^{-1} band which remains above the transition temperature is an asymmetric methylene stretching mode. The presence of the 2880 cm^{-1} band in the range of 24–37°C, in the recombinant, indicates that some of the phosphatidylcholine chains are still ordered, so that the resonance-enhanced 2880 cm^{-1} dominates this region of the spectrum.

Curatolo et al. [78] have previously used model-building arguments to show that a 'boundary layer' extends out from dimyristoyl phosphatidylcholine-proteolipid apoprotein complexes in 3–4 concentric annuli at the phase transition, but could not derive an estimate of the size or state of this 'boundary layer' at higher temperatures. However, the Raman CH-stretching data indicate that, at temperatures above that at which the calorimetrically-observed, cooperative transition is complete, the dimyristoyl phosphatidylcholine acyl chains still possess some solid character. In addition, the difference in $[I_{\approx 2890}/I_{\approx 2850}]$ between the complex and pure dimyristoyl phosphatidylcholine decreases with increasing temperature, indicating that the effective size of the 'boundary layer' declines with increasing temperature in the liquid-crystalline state. This behavior indicates that in the liquid-crystalline state, one is not really observing a 'boundary layer' but a 'boundary gradient'. In such a gradient, acyl chain fluidity will increase as the distance from the apolar protein perimeter increases, as originally proposed by Wallach and Gordon [79]. However, as the temperature is raised, the outer layers of the 'boundary gradient' disorder progressively increase in fluidity, approaching the state of free dimyristoyl phosphatidylcholine. The layers of the gradient closest to the protein also increase in fluidity, at least up to 40°C, but do not become as fluid as free phosphatidylcholine. These results fit the recent model on lipid-protein interactions by Marcelja [80], predicting 4–5 layers of bound lipid around hydrophobic proteins at temperatures near, but above, that of the lipid phase transition and a decrease in the size and order of this boundary layer with increasing temperature.

The behavior of the egg phosphatidylcholine-proteolipid apoprotein recombinant in the CH-stretching region is more complex than that of the dimyristoyl phosphatidylcholine-proteolipid apoprotein recombinant, presumably because of the heterogeneous acyl chains of this phospholipid. Firstly, proteolipid apoprotein broadens the main thermotropic transition (–6°C). Secondly, a new biphasic transition, appears with an inflection point at 12°C, also shown by differential scanning calorimetry, representing a cooperative structural transition. We suspect that proteolipid apoprotein has stabilized a population of phosphatidylcholine molecules in a rigid state, preventing their order-disorder transition until 12°C. The remainder of the egg phosphatidylcholine molecules undergoes a severely perturbed transition, spanning a temperature range from –26°C to 10°C. A simple interpretation for this complex behavior is not yet possible. Conceivably,

proteolipid apoprotein preferentially binds acyl chains of a particular length or degree of unsaturation, thus leading to a particular chemical structuring of the 'boundary gradient' surrounding the protein. Since $[I_{\approx 2880}/I_{\approx 2850}]$ of the egg phosphatidylcholine-proteolipid apoprotein complex is greater than in pure egg phosphatidylcholine it is possible that, at these temperatures, the acyl chains of the complex are in a more rigid state than without proteolipid apoprotein. In any event, even the minor complexity of chain heterogeneity in egg phosphatidylcholine (principally palmitoyl and oleoyl phosphatidylcholine) appears to create a situation where some of the phospholipid sequestered by the protein into regions which can undergo cooperative thermal transition at a temperature 20°C higher than the normal crystal ⇌ liquid crystal transition. Analogous patterns are to be expected in biomembranes where there is greater protein and lipid heterogeneity than here.

IXB. Phosphatidylcholine-cytochrome oxidase and phosphatidylcholine-cytochrome c

Our studies on proteolipid apoprotein-phosphatidylcholine recombinants relate to those of Lis et al. [21] on complexes of cytochrome oxidase with dimyristoyl and dipalmitoyl phosphatidylcholine multilayers at weight ratios of 4 : 1 (protein/lipid). Cytochrome *c*/phosphatidylcholine mixtures were used as models for the interaction of 'extrinsic' membrane proteins with phospholipid bilayers. The authors find a lower $[I_{2890}/I_{2850}]$ for phosphatidylcholine in the presence of both cytochrome oxidase and cytochrome *c*. Unfortunately the authors were not able to measure transition temperatures or ratio changes over the transition ranges, and thus could not detect possible shifts in these important variables. However, their data indicate that cytochrome oxidase, like proteolipid apoprotein tends to disorder the lipid acyl chains below the phosphatidylcholine transition temperature.

X. Biomembranes

XA. Introduction

Plasma membranes isolated as small, sealed vesicles have proven very suitable for Raman analyses, as have sarcoplasmic reticulum vesicles. Good Raman spectra have also been obtained with intact erythrocyte ghosts. Qualitatively the spectra obtained are on the whole what one would expect from protein-lipid composites. Quantitative analyses, however, have provided important insights into the structural dynamics of proteins and lipids in biomembranes.

XB. Membrane proteins

XB (1). Secondary structure

As summarized by Lippert et al. [81] and Koenig [82], several of the amide bands of proteins and polypeptides exhibit conformational sensitivity. Accordingly, Lippert et al. [81] developed a technique for the determination of protein secondary structure by Raman spectroscopy. For this they obtain spectra in H_2O and ^2H_2O, of polylysine in its α-helical, antiparallel β and unordered (U) states, as well as of lysozyme and ribonuclease A (proteins of known secondary structure). The intensities of the amide III bands at 1240 cm^{-1} (H_2O) as well as of the amide I′ (^2H_2O) bands at 1660 and 1632 cm^{-1} were measured using the HCH deformation band near 1450 cm^{-1} as internal reference.

The authors propose that the conformational composition of unknown proteins can be determined from four simultaneous equations:

$$C_{\text{protein}}\, I_{1240}\text{-protein} = f_\alpha\, I_{1240}\alpha + f_\beta\, I_{1240}\beta + f_U\, I_{1240}U$$

$$C_{\text{protein}}\, I_{1632}\text{-protein} = f_\alpha\, I_{1632}\alpha + f_\beta\, I_{1632}\beta + f_U\, I_{1632}U$$

$$C_{\text{protein}}\, I_{1660}\text{-protein} = f_\alpha\, I_{1660}\alpha + f_\beta\, I_{1660}\beta + f_U\, I_{1660}U$$

$$1.0 = f_\alpha + f_\beta + f_U$$

Here, C is an experimentally defined scaling factor relating the intensity of the HCH-bending band of a protein to that of poly-L-lysine. For proteins of known crystal structure C ranges from 0.65 to 0.95. I_{1240}-protein is the scattering intensity at 1240 cm^{-1} of the unknown protein (in an H_2O medium) relative to the HCH-bending intensity; $I_{1240}\alpha$ is the value for pure α-helix, i.e. helical poly-L-lysine.

Taking, f_α, f_β and f_U to constitute the fractions of α-, β- and unordered (U) peptide in the protein and applying these factors plus appropriate scaling values, C, for proteins with secondary structures determined by X-ray crystallography, Lippert et al. [81] obtained the relative I values listed in Table I.

The results presented indicate that the equations presented and values given in Table I would allow the conformational analysis of unknown proteins to within ±15% provided that (a) right-handed α-helix, β-structure and unordered structures are the only conformations present, and (b) that solution or membrane structures of proteins do not deviate drastically from crystal structures.

Unfortunately, published reports indicate that the approach of Lippert et al. [81] has not yet been applied to biomembranes or isolated membrane proteins.

XB (2). Side chain amidation

In their studies on plasma membranes of concanavalin A-stimulated lymphocytes, Schmidt-Ullrich et al. [26] noted a series of sharp bands on the low frequency side (1660 cm^{-1}) of the broad amide I-water peak, bands not observed with membranes from unstimulated cells. By reference to a series of simple amides, these peaks could be tentatively assigned to the amide I and II bands of side chain asparagine and glutamine. This assignment, confirmed by isoelectric focussing, implies lesser post-synthetic deamidation of the stimulated cells' plasma membrane proteins. Verma et al. [29] have observed increased side chain amidation also in the plasma membrane proteins of hamster lymphocytes (GD248) neoplastically transformed by simian virus 40, compared with normal resting lymphocytes. In this report too support for the Raman assignments was obtained

TABLE I

RELATIVE RAMAN INTENSITIES I^α, I^β, AND I^U

	1240 cm^{-1} (H_2O)	1632 cm^{-1} (^2H_2O)	1660 cm^{-1} (^2H_2O)
α-Helix	0.00	0.80	0.55
β-Structure	1.20	0.72	0.88
Unordered	0.60	0.08	0.78

Modified from Ref. 81.

by isoelectric focussing. Conceivably high plasma membrane protein side chain amidation is a characteristic of activated lymphocytes.

XB (3). Conformational analyses of membrane proteins

At the present no rigorous explorations of average membrane protein conformation by Raman spectroscopy have appeared, although several workers have qualitatively reported on this matter.

Thus, in our earlier work [24] we examined membranes of human erythrocytes in H_2O and ^2H_2O. On the basis of the amide I and III intensities, we diagnosed the presence of α-helix and unordered structures but could not give a quantitative estimate of average secondary structures. In contrast, Lippert et al. [23], also working with 'ghosts' of human erythrocytes arrived at an estimate of "40–55% α-helix with little β-configuration". This estimate used poly-L-lysine as reference for the amide III intensity in H_2O and the amide I′ bands in ^2H_2O. More recently, Milanovitch et al. [30] working with membranes from Dutch belt rabbit erythrocytes, estimated 'considerable α-helix' on the basis of the amide I and III intensities, but point to a slight shoulder at 1645 cm^{-1}, suggesting β-structure. Overall, therefore, Raman data on resting, unperturbed erythrocyte membranes indicate considerable α-helix and little β-structure.

Two reports also deal with the average conformational status of plasma membranes of rabbit thymocytes. Verma et al. [25] reasoned on the basis of a 1660 cm^{-1} amide I band and the distinct amide III banding at 1228 cm^{-1} and 1240 cm^{-1}, that these membranes' proteins contain appreciable β-structured peptide backbones. This conclusion was confirmed by infrared spectroscopy. No β-structure was noted in endoplasmic reticulum membranes of thymocytes. A subsequent study by Schmidt-Ullrich et al. [26] on membranes of concanavalin A-stimulated thymocytes was possibly consistent with a greater proportion of β-structure.

In their study on the sarcoplasmic reticulum membranes of lobster muscle, Milanovitch et al. [31] report an amide III shoulder at 1246 cm^{-1} "possibly indicative of β or random coil structure" They could not analyze the amide I or I′ region due to a very strong ν(C=C) *cis* band at 1658 cm^{-1};

Finally, Rothschild et al. [32] in their report on isolated bovine opsin, conclude that this protein is highly helical and contains little or no β-structure.

XB (4). Comparison of intact and peripheral protein-free erythrocyte ghosts

Recently, Goheen et al. [83] compared the Raman spectra of intact erythrocyte ghosts with vesicles free from peripheral proteins. The Raman spectra in the 900–3000 cm^{-1} region were very similar to spectra presented earlier [23,24]. The intensities of various bands arising from both lipids and proteins were compared. The band at 1440 cm^{-1} was used as an internal standard because (a) there is no loss of lipid during extraction, (b) peripheral proteins contribute only 12% of the height of this band, and (c) there is no change in the conformation of membrane lipids upon extraction. Normalized ratios, i.e. the ratio of peak heights of Raman features from extracted membrane preparations (I_{12}) and of normal membrane preparation (I_n), I_{12}/I_n, deviated from unity upon change in environment. Changes of I_{12}/I_n to 1.8 and 1.7 for ring vibrations at 1005 and 1030 cm^{-1}, respectively, were taken to indicate modifications in the tryptophan and phenylalanine ring environments of the depleted erythrocyte ghosts. However, it is dangerous to assign the 1006 or 1002 cm^{-1} band to Trp and Phe rings exclusively because β-carotene, associated with the membrane, gives a strong band in this region. (Its intensity quenches

upon longer irradiation.) Also the 1030 cm^{-1} band is weak for quantitative studies.

Changes observed in the lower part of the amide I and 950 cm^{-1} regions were more impressive. In the former, peaks assigned to Trp and Phe resolved at 1622, 1605, and 1586 cm^{-1} upon extraction. These lie under a broad shoulder in the native membrane preparation. The 950 cm^{-1} band, assigned no C–C-stretching of the peptide backbone, split into two weak bands, 926 and 960 cm^{-1}. These observations suggest that the extraction procedure of peripheral proteins changes the environment of peptide bonds as well as of phenylalanine and tryptophan rings of integral membrane proteins.

Examination of I_{12}/I_n for lipids in the CH-stretching region did not show any appreciable deviation from unity in the extracted membranes. However, data on the C–C-stretching region (1100 cm^{-1}) appear contradictory. The $[I_{1130}/I_{1085}]$ ratio increased while $[I_{1065}/I_{1085}]$ remained unchanged. Goheen et al. [83] argue that membrane proteins may contribute to the 1100 cm^{-1} region, accounting for an unexpected increase in $[I_{1130}/I_{1080}]$. However, an examination of the Raman spectra of standard and extracted ghosts suggests that it is difficult to reliably measure the height of the 1130 cm^{-1} peak *. The 1130 cm^{-1} band is close to the strong β-carotene band at 1159 cm^{-1}. The 1159 cm^{-1} band appears to be weak in the standard ghosts while it is strong in the extracted sample, perhaps due to the difference in irradiation times before the spectra were recorded.

XC. Protein state transitions

XC (1). Erythrocyte membranes

Verma and Wallach [28] have examined the CH-stretching region of erythrocyte ghosts as a function of temperature and pH. They find that, at 22°C, the CH-stretching region is characterized by three strong bands that lie at approx. 2930, 2880, and 2850 cm^{-1}. As the temperature is raised from about 22 to above 42°C at pH 7.4, the ≈2930 cm^{-1} band becomes very prominent, relative to the temperature-insensitive feature at 2850 cm^{-1}, and the ≈2880 cm^{-1} peak becomes obscured. Fig. 11 describes plots of $[I_{2930}/I_{2850}]$ vs. temperature. At pH 7.4 $[I_{2930}/I_{2850}]$ stays stable at approx. 1.2 ± 0.02 between set temperatures of 20 and 35°C and then abruptly shifts to about 1.41 between set temperatures of 36 and 45°C. This transition is reversible only up to a set temperature of 39°C. Correcting for the local heating due to the laser beam gives a lower temperature limit of 38°C for the discontinuity and an irreversibility temperature of 42°C.

Reduction of pH modifies the temperatures and magnitudes of the high-temperature discontinuities in $[I_{2930}/I_{2850}]$. No significant change occurs between pH 7.0 and 7.5 (Fig. 11). However, at pH 6.5 the transition is centered at a corrected temperature of about 31°C with a lower limit near 22°C (corrected). As the pH is reduced to 6.0, the transition range drops to 0–7°C (corrected) with a range in $[I_{2930}/I_{2850}]$ of approx. 1.0–1.35.

The data clearly indicate that the transition reported by the change of $[I_{2930}/I_{2850}]$ can be brought about isothermally by a small change of $[H^+]$ in the physiological pH range. Indeed, an increase in $[H^+]$ of about 0.6 μM, (pH $7.0 \rightarrow 6.5$) corresponds to a 16°C lowering of transition temperature.

The effects of temperature and pH on Raman scattering closely correspond to those

* Possibly the baseline for height measurement differed between standard and extracted ghosts due to the closeness of the 1130 cm^{-1} band to a strong β-carotene band at 1159 cm^{-1}.

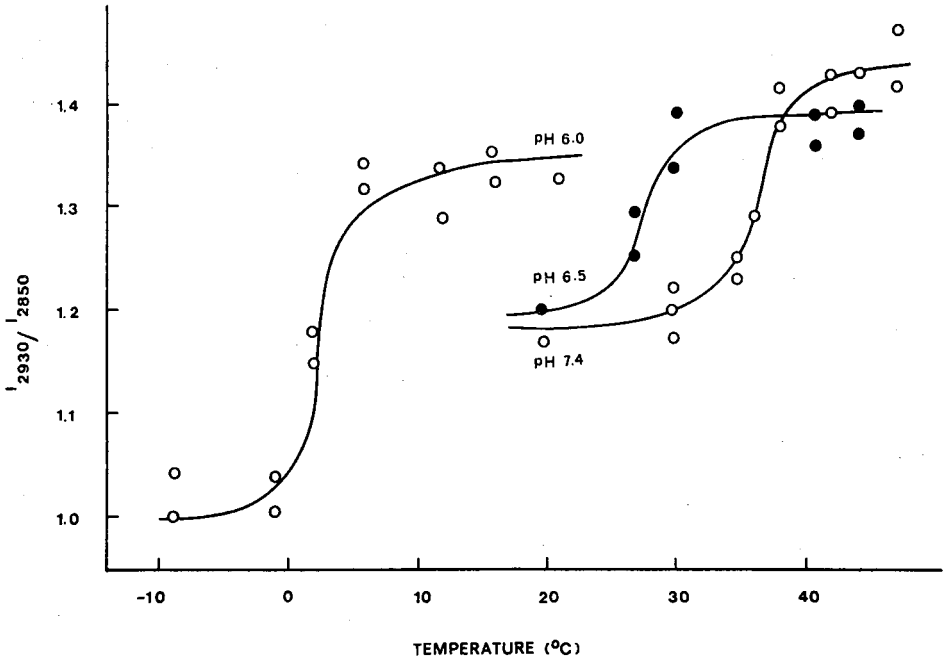

Fig. 11. Variation of $[I_{2930}/I_{2850}]$ of erythrocyte ghosts with temperature, at pH 6.0, 6.5, and 7.4, respectively. From Ref. 28, with kind permission from the National Academy of Sciences, Washington, D.C.

detected by studies on the interaction of membrane protein fluorophores and lipid-soluble fluorescence quenchers [84]. Earlier [28] we pointed out that >60% of the Raman scattering ≈2930 cm^{-1} is due to protein and suggested that (a) the apolar residues of penetrating proteins, together with the hydrocarbon chains of phospholipids immediately apposed to these protein residues, constitute a separate phase, (b) the high-temperature, pH-sensitive thermotropic step in $[I_{2930}/I_{2850}]$ represents a cooperative state transition in this phase, involving a concerted rearrangement of acyl chain configuration and protein residue orientation. In this, we propose that the pH susceptibility of the thermosensitive $[I_{2930}/I_{2850}]$ discontinuity may relate to the reversible thermotropic transitions observed in some soluble globular proteins at pH values below their isoelectric points. We propose that the large response in the pH range 7.0–6.0 might derive from the low dielectric constant of the membrane core: small changes in charge might influence the structure of proteins in membranes much more than that of proteins dissolved in aqueous solvents.

XC (2). Plasma membranes from normal hamster lymphocytes and lymphoid cells neoplastically converted by simian virus 40

The high temperature thermotropism of plasma membrane vesicles isolated from normal and neoplastic (simian virus 40-induced) hamster lymphocytes has been compared [29]. No changes in $[I_{\approx 2880}/I_{2850}]$, or the acoustical regions were observed above 20°C. However, very significant changes were noted in $[I_{\approx 2930}/I_{2850}]$, which is stable below 10°C (Fig. 12). In the case of membranes from normal cells, this ratio remains stable to a set temperature of 37°C. At slightly higher temperatures, $[I_{\approx 2930}/I_{\approx 2850}]$

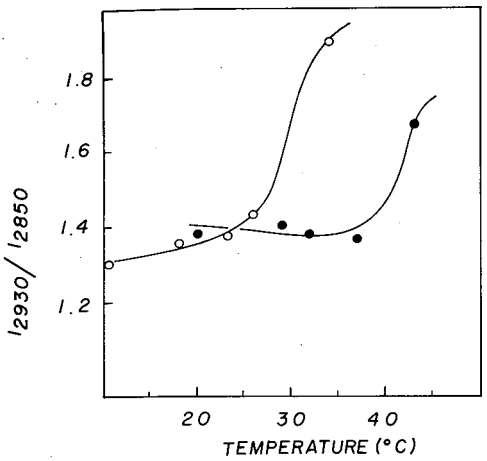

Fig. 12. Plasma membrane from normal and neoplastic lymphocytes. Variation of $[I_{2930}/I_{2850}]$ with temperature. •, membrane from normal cells; ○, membranes from neoplastic lymphocytes, GD248 cells. The abscissa gives set temperatures. Calibrations show that sample temperatures are 2°C higher at 20°C and 3°C higher at 40°C. Points marked in the curves represent averages for 5–7 different membrane preparations. The maximum range of variation at a given temperature is ±6%. From Ref. 9, with kind permission from The University of Chicago Press, Chicago, IL.

increases abruptly up to 43°C. At temperatures slightly above 43°C, the bands in the CH-stretching region become too broad to yield reproducible intensity ratios.

Tumor cell membranes differ dramatically (Fig. 12). While $[I_{2930}/I_{2850}]$ is stable up to 23°C (set temperature), it increases abruptly at slightly higher temperatures, reaching a limit at 34°C; beyond this, no satisfactory intensity ratios could be obtained.

We propose [29] that the thermotropism of $[I_{\approx 2930}/I_{2850}]$ observed with lymphocyte membranes has the same explanation as forwarded above for erythrocyte membranes. However, the membranes from neoplastic cells at a sample temperature of ≈37°C are in a state achieved by normal membranes at 47°C. We propose that abnormal proteins, shown to exist in the tumor-cell membranes, might account for the abnormal thermotropism observed.

XD. Membrane lipids

XD (1). Composition

All membranes studied exhibit the lipid chain contributions to the CH-stretching, CH-deformation, skeletal-optical and acoustical regions already discussed for lipid systems. However, these can be clearly discerned from protein contributions only in the CH-stretching and acoustical regions. However, the spectra of diverse membranes can indicate differences in lipid composition.

Thus, the plasma membranes of human erythrocytes [12,23,24], thymocyte endoplasmic reticulum [25] and lobster sarcoplasmic reticulum [31] clearly contain traces of conjugated polyenes, yielding resonance-enhanced Raman bands at approx. 1530 and 1165 cm^{-1} attributable to ν(–C=C–) and ν(=C–C=) of carotenoids. The environmental sensitivity of these bands has already been discussed.

Membranes of human erythrocytes in ^2H_2O exhibit a band at 1655 cm^{-1} not definitively assigned initially [24] but probably representing ν(C=C) of *cis*-unsaturated

phospholipid double bonds. A poorly resolved band displayed at 1659 cm^{-1} by erythrocyte membranes of Dutch belt rabbits in H_2O [30] may have the same origin.

In lobster sarcoplasmic reticulum the ν(C=C) *cis* band is very prominent [31] at 1658 cm^{-1}, suggesting a high level of acyl chain unsaturation. This is also evident from a HC=CH CH-stretching band at 3016 cm^{-1}, and Milanovitch et al. [31] propose that there might be CH-stretching contributions above 2900 cm^{-1} due to short $(CH_2)_n$ segments separated by C=C bonds. That this is likely is indicated by recent studies on unsaturated fatty acids [5].

The plasma membranes from concanavalin A-stimulated thymocytes, unlike the membranes from quiescent cells, show a prominent Raman scattering band at 1655 cm^{-1} [26]. This persists in ^2H_2O and has been assigned to ν(C=C) of *cis*-unsaturated double bonds. This difference between resting and stimulated cells is not unanticipated, since the latter's phospholipids are known to be more highly unsaturated. In view of recent information [5] the greater plasma membrane acyl chain unsaturation of the stimulated cells may also account for the greater $[I_{\approx 2880}/I_{2850}]$ (6.6 vs. 1.3 for quiescent cells), and the different structure of the HCH deformation region [26].

XD (2). Lipid state transitions

XD (2) a. Erythrocyte membranes. We [27] have examined the Raman scattering from erythrocyte ghosts at 2700–3000 cm^{-1}, that at low frequencies due to acoustical vibrations, as well as that due to ν(–C=C–) and ν(=C–C=) of β-carotene, in the temperature range of –30 to 30°C. Liposomes composed of phosphatidylcholines ± cholesterol were used as controls. We found (Fig. 13) that, in the case of erythrocyte membranes, plots of $[I_{\approx 2930}/I_{2850}]$ and $[I_{\approx 2880}/I_{2850}]$ against temperature exhibit multiple discontinuities. Thus, $[I_{2932}/I_{2850}]$ rose from a value of 1.03 ± 0.02, stable below –20°C, to a value of 1.15 ± 0.07, stable to 30°C, with a half-maximal change at –3°C. In contrast, the variation of $[I_{2880}/I_{2850}]$ with temperature was biphasic, beginning below –20°C and extending to approx. 4°C (1.17 ± 0.05). It was half-maximal below –8°C and approximately followed the $[I_{\approx 2932}/I_{2850}]$ transition. The second discontinuity, from 1.15 ± 0.05 to 1.00 ± 0.03, occurred between 14 and 20°C (half-maximal at 15°C). The second decrement in $[I_{\approx 2880}/I_{2850}]$ was associated with a change of $[I_{1527}/I_{1158}]$ from 1.3–1.4. to 1.0–1.1. In contrast $[I_{1527}/I_{1158}]$ did not change between –30 and 14°C. It is suggested, therefore, that the β-carotene in erythrocyte membranes is restricted to the lipid domains undergoing a state of transition between 14 and 20°C. The direction of change of $[I_{1527}/I_{1158}]$ in this temperature range corresponds to that accompanying gel → liquid-crystal transitions in phosphatidylcholine liposomes doped with β-carotene [12].

Correcting for local heating due to the laser beam, we [27] arrived at the following 'transition' temperatures: –3°C ($[I_{\approx 2932}/I_{2850}]$) below –4°C, (first step in $[I_{\approx 2880}/I_{2850}]$) and 17°C (second $[I_{\approx 2880}/I_{2850}]$ step).

Fig. 14 shows the acoustical region of erythrocyte membranes at several temperatures. The spectrum at 2°C, as well as those obtained at higher temperatures, is remarkable for its lack of detail compared with the spectrum of phosphatidylcholine liposomes and even cholesterol-phosphatidylcholine liposomes. At –1°C shoulders emerge at 255, 232, and 210 cm^{-1}. These are thought to indicate crystallization of unsaturated chains, which, according to the changes in the CH-stretching region should be in progress at this temperature. In the –6°C spectrum, the interval between 230 and 190 cm^{-1} is obscured by the ice I peak, but there is no indication of any structuring at frequencies expected of the acoustical modes of unsaturated or saturated acyl chains. However, such does emerge at

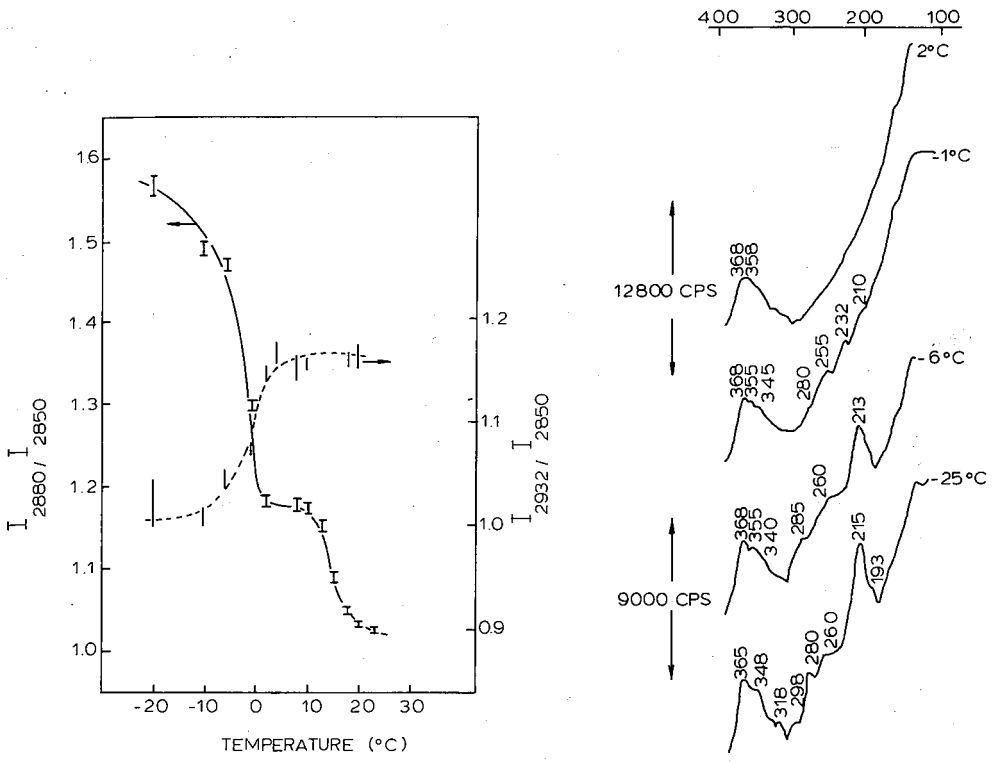

Fig. 13. Variation with temperature of $[I_{\approx 2880}/I_{2850}]$ (left ordinate) and $[I_{2932}/I_{2850}]$ (right ordinate) of erythrocyte membranes. ———, $[I_{2880}/I_{2850}]$; - - - - - -, $[I_{2932}/I_{2850}]$. The bars give ranges of experimental values. From Ref. 27.

Fig. 14. Raman spectra in the acoustical region of erythrocyte membranes at various temperatures. From Ref. 27.

–25°C (bands at 318, 298. 280 cm^{-1}, a sharp shoulder at 260 cm^{-1} and a weak shoulder at approx. 193 cm^{-1}). The low temperature response of the erythrocyte membranes thus resembles that of phosphatidylcholine-cholesterol liposomes and may derive, at least in part, from their high cholesterol content. In terms of the previously described properties of model systems, one might ascribe the discontinuity in $[I_{\approx 2880}/I_{2850}]$ vs. temperature near 17°C (corrected temperature) to a crystal ⇌ liquid-crystal transition in a region of low cholesterol content (⩽6 mol%). The fact that this transition corresponds to the abrupt decrement of $[I_{1527}/I_{1158}]$ of membrane-bound β-carotene would fit the suggestion that a low cholesterol region is involved since β-carotene appears excluded from cholesterol-rich domains. Similarly, one might well attribute the broader steps in $[I_{\approx 2880}/I_{2850}]$ and $[I_{\approx 2932}/I_{2850}]$ to crystal ⇌ liquid-crystal transition in domains of higher cholesterol content. However, other thermally-induced rearrangements of lipid architecture, e.g. phase segregation, may also be involved.

The above-described Raman data, and their interpretation, appear to resolve some apparent inconsistencies between results obtained by other techniques. Thus erythrocyte membranes exhibit no thermotropic lipid phase transitions that can be detected by differential thermal calorimetry [85] or X-ray analyses [86]. Also, erythrocyte mem-

brane proteins lack significant mobility in the plane of the membrane [87] and appear to restrain the mobilities of membrane lipids [88,89]. Moreover, the X-ray experiments of Gottlieb and Eanes [86] on hydrated erythrocyte membrane lipids, depleted of cholesterol to varying extents show that with 6 mol% cholesterol, crystal and liquid-crystal states can coexist between 2 and 20°C, although liquid-crystal domains predominate already at −10°C, and at higher cholesterol proportions only the liquid-crystalline state is detected even at −20°C. Concordant information has been reported by Jackson et al. [90] who found no calorimetrically detectable phase transition in hydrated membrane lipids unless 81% of the cholesterol was removed. Then a very broad transition (5–45°C), centered at 25°C, was observed. However, Zimmer and associates, [91,92] describe a thermotropic viscosity change, discontinuous at 18–20°C, in erythrocyte membranes, as well as cholesterol-depleted membrane lipids and correlate this with the discontinuity at 19°C in the Arrhenius plot for glucose transport [93]. Recent ESR studies of normal erythrocyte ghosts labeled with nitroxide fatty acids demonstrate a thermal transition at 13–16°C and a pH-sensitive transition at 37.5–40.5°C [94]. Similarly, Hui and Strozewski [95], using electron diffraction studies of erythrocyte membranes, noted a thermal transition at -3 ± 3°C in both fresh membranes as well as in their total lipid extracts. One explanation for these apparently inconsistent observations is that the diverse experimental approaches monitor different properties of a composite membrane, where a number of microdomains coexist.

XD (2) b. Thymocyte plasma membranes. A plot of $[I_{\approx 2890}/I_{2850}]$ vs. temperature of highly purified thymocyte plasma membrane vesicles shows a marked discontinuity centered at about 21°C (corrected temperature [25]). $[I_{\approx 2890}/I_{2850}] = 1.3$ at 22°C and 2.2 at 10°C. This discontinuity, although less broad than observed in phosphatidylcholine liposomes (1 : 1, mol/mol) still suggests a lesser degree of cooperativity than is observed in phosphatidylcholine liposomes. It may represent a lipid phase transition or a lipid phase segregation phenomenon in a low cholesterol domain. No thermotropism could be detected in the protein-dominated C–C-stretching region and the acoustical region was not studied.

XD (2) c. Plasma membranes of normal hamster lymphocytes and membranes of lymphoid cells neoplastically transformed by simian virus 40. Plots of $[I_{\approx 2880}/I_{2850}]$ vs. temperature, as well as of the half width of the ≈ 2880 cm^{-1} band vs. temperature (Fig. 15) for membranes of normal cells show a symmetrical discontinuity centered at about 7°C and approx. 5°C wide [29]. $[I_{\approx 2880}/I_{2850}]$ for membranes of neoplastic lymphocytes, in contrast, reveals a broader discontinuity between 2 and −10°C. The half-width measurements indicate a change beginning at 10°C, centered at −5°C and complete at −10°C. Analyses of the acoustical region yielded concordant results: thermosensitive spectral changes consistent with crystal ⇌ liquid-crystal transitions were noted in both membrane categories, but those of the neoplastic cells occurred at much lower temperatures. The data indicate that the plasma membrane acyl chains of neoplastic and normal cells undergo state transition at low temperature but that the former is less cooperative than the transition of normal membranes. The CH-stretching data, as well as analyses of the acoustical region, further show that the transition temperature for the membranes of neoplastic cells is at least 12°C lower than normal. In both cases, the direction of the CH-stretching and acoustical changes are those of poorly cooperative gel ⇌ liquid-crystal transitions, that of the neoplastic cell membranes being least cooperative.

The different lipid thermotropisms of membranes from normal and neoplastic lymphoid cells might represent the composite contributions of acyl chain unsaturation,

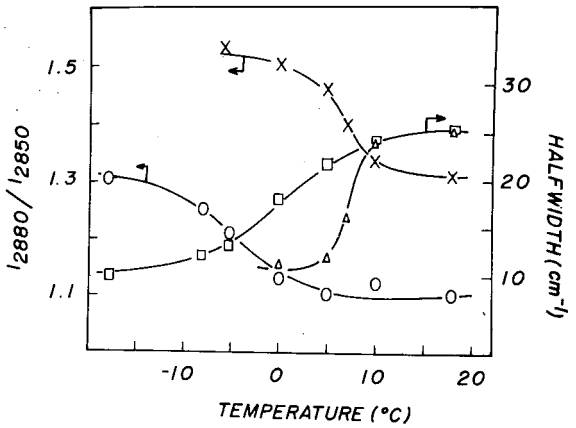

Fig. 15. Plasma membranes from normal and neoplastic lymphocytes. Variation of $[I_{\approx 2880}/I_{\approx 2850}]$ (left ordinate) and half-width of the 2880–2890 cm^{-1} band (right ordinate) with temperature. X and △, points for membranes from normal cells; ○ and □, points for membranes from neoplastic lymphocytes from GD248 cells. The abscissa gives set temperatures. Calibrations show that the sample temperatures are at most 1°C higher at 0°C. Each point is an average computed from the spectra of 5–7 different membrane preparations. Maximum range of variation at each temperature is ±6%. From Ref. 29, with kind permission of the University of Chicago Press, Chicago, IL.

cholesterol distribution, and the presence in the transformed cells' membranes of abnormal simian virus 40-coded protein (cf. Section XC (2)).

XI. Infrared spectroscopy

XIA. Introduction

As previously indicated [96], Raman scattering and infrared absorption methods are largely complementary; vibrational bands that are intense in the scattering spectrum often produce weak absorptions, and conversely many biomolecules possess significant modes which can only be observed in the infrared. In particular, the polar head group vibrations of phospholipids, the amide motions of polypeptides and the modes of free and bound water (and other hydrogen-bonded species) absorb strongly and significant studies exist in these areas [97–99]. Infrared work also exists involving the CH-stretching and bending modes of aliphatic chains to monitor phase transitions of phosphatides [100] and to deduce crystal packing in lipid multilayers [97]. In addition, several theoretical papers have recently appeared which treat the conformationally-sensitive amide bands of polypeptides [101,102] and the Fermi-resonance interaction between methyl bending and stretching modes in the infrared spectrum [42]. These last works provide a firm basis for the interpretation of studies in lipid phase transitions and protein conformation changes. Furthermore, new preparative and instrumental methods exist which partially circumvent a primary difficulty in the infrared spectroscopy of aqueous biological samples, the broad intense absorptions of water which can easily obscure other bands. This section evaluates the progress in the above areas and details the special techniques useful in the infrared

spectroscopy of biological systems. The technical discussion includes methods of sample preparation, temperature control, data analysis, and describes a simple way of obtaining dichroic ratios for partially-ordered systems [99]. We also mention a technique for synchronous modulation and detection of infrared absorption bands which may have wide use [103]. The review concerns primarily the fundamental region in the infrared from 4000–200 cm^{-1}; however, we indicate the possibilities for experimentation in the far-infrared (200–10 cm^{-1}). This latter region, which includes the collective modes of long chains and crystalline lattices may prove important since these modes have possible functional significance in biomembranes.

XII. Technical

XIIA. Instrumentation

Conventional infrared absorption spectra of bio-samples may be obtained with many commercial infrared spectrometers. Most modern instruments are dual-beam monochromators that electronically or optically match the intensities of the sample and reference beams to measure the sample absorption. Dual-beam operation reduces problems due to wavelength-dependent variations in source intensity or detector sensitivity. Furthermore, the existence of separate sample and reference signals makes the recording possible of differences between spectra of specimens placed in the two beams. Difference spectra are valuable in the compensation of solvent absorptions (particularly those of water) and in the detection of small differences between almost similar systems. Thus, Asher and Levin [100] obtained good spectra of aqueous dispersions of phospholipids by using a matched cell containing only water in the reference beam.

Most modern infrared spectrometers may be operated with either fixed slit widths or with the slits programmed to maintain approximately constant energy at the detector throughout the frequency range of the instrument. In either case, the entire optical path must be purged to remove water vapor and carbon dioxide. Although dual-beam photometers should ideally compensate for atmospheric absorption, such compensation fails if the sample and reference beams have different path lengths in the air (as with a thick sample). Furthermore, at long wavelengths the source intensity falls rapidly and the atmospheric absorption in this range may reduce the signals to a point where the servomechanisms of optical null spectrometers can no longer respond. Purging is best achieved with a flow of dry nitrogen (although exposure to a pure nitrogen atmosphere may shorten the lifetime of some infrared sources [104]). There also exist commercial, continous duty air driers which can be connected to a compressed air supply (at about 80 lb/inch) to provide a constant flow of dry air (at about 1 $foot^3$/min) for purging. These units may also absorb CO_2 and typically will reduce water vapor to insignificant amounts and CO_2 by a factor of 5–10 within 30 min [104].

Spectrometers for use in the far-infrared region employ gratings as the dispersive elements (e.g. Perkin-Elmer model 180 with far-infrared option) or are non-dispersive instruments (e.g. Beckman RIIC FS700 Fourier spectrometer). Compared with dispersive measurements Fourier-transform spectroscopy yields the same improvements in signal intensity (or reduced data collection times) as does multiplex Raman spectroscopy (see Section IIB). Thus, such units are preferable for biomembrane work in the far infrared where water absorptions are even more problematic than in the fundamental region [106].

Suitable window materials are scarce. Cesium iodide, the longest wavelength transmitting alkali halide, may be used in windows to about 50 μm. Satisfactory substrates are polyethylene, Teflon or TPX (polymethyl-4-pentene-1) [107]. The only inorganic substance that transmits throughout the far-infrared is diamond which finds use in micro optics and as a detector window.

The potential of the far infrared region to structural analysis of biomembrane components seems large, since the collective modes of macromolecules fall in the range. For example, Bertz and Ascarelli [107] have obtained spectra of poly(I) · poly(C) RNA in the 150–20 cm^{-1} region which clearly reflect the A–A′ structural transition (between 11- and 12-fold helices, brought about by changing NaCl concentration). These spectra show a broad band, assigned to collective stretching of the interchain H-bonds, that shifts from 40 to 70 cm^{-1} at the A–A′ transition. We know of no application of these methods to biomembrane studies.

Bertie and Whally [108] present the far-infrared spectra of ices Ih and Ic in the range of 360–50 cm^{-1}. These data, along with the included theoretical discussion of lattice modes of orientationally disordered crystals may be useful to studies of structured membrane water.

XIIB. Sample preparation

Proper sample preparation is essential to the infrared spectroscopy of biological materials. Substances that can be deposited as films or layers on an appropriate substitute are probably best examined in that form, since films permit good control of temperatures and hydration. We thus concentrate on film technique; however, we also mention the use of pressed potassium bromide discs, and a new method of embedding phospholipids in a clay matrix [105] for infrared studies.

XIIB (1). Films

Films may be formed directly on various substrates by evaporation from aqueous or organic solvents, by solidification from a melt or by drying of aqueous suspensions. Although many infrared transparent windows exist, we [97] have found that silver bromide has the greatest general usefulness and is transparent throughout the entire fundamental infrared from 4000 to 250 cm^{-1}, insoluble in water and most organic solvents, and available in many sizes and thicknesses [109]. The material is soft and somewhat fragile; but scratched surfaces may be repolished by soaking in a 50% butylamine/ethanol mixture and buffing with a soft cloth. Because AgBr is slightly ultraviolet photosensitive, AgBr windows are best stored in the dark. However, AgBr is less problematical than AgCl (which transmits only to about 400 cm^{-1}). The AgBr surfaces are strongly hydrophobic, but slight roughening of the surface by buffing with lens tissue improves the wettability considerably, and we [110] have had no difficulty in spreading aqueous suspensions of mitochondria on plates prepared in this manner (Fookson, J. and Wallach, D.F.H., unpublished results). AgBr has a low thermal conductivity. For temperature control, it is therefore important to use heat transfer surfaces that are as large as possible and to measure the sample temperature on the window (but outside the beam) (see Section IIC (1)). A potentially very useful technique for the infrared spectroscopy of membrane components is the freeze-drying of aqueous suspensions which are spread over the plate, quickly frozen in liquid nitrogen and then dried. Thus, Wallach and Graham [110] prepared 'films' of mitochondrial membranes by lyophilization of the frozen sam-

ples applied directly onto the windows. We [110] have later found that slower sublimation in a dry atmosphere at −20°C (simply by storing the frozen samples overnight in a cold room) yields more cohesive films that scatter much less of the incident infrared than those prepared by vacuum drying. Importantly, the films may then be rehydrated and examined with the minimum amount of water necessary for biological functioning. In addition, the rapid freezing of the preparation permits kinetic studies, since biological reactions may be halted at a particular instant. Studies have further shown that drying and subsequent careful rehydration do not necessarily destroy membrane function; thus mitochondrial membranes treated in this way retain their ability for coupled respiration.

We [97] have achieved controlled rehydration of phospholipid films as in Ref. 112 by placing the films in a dessicator over various saturated salt solutions (appropriate compounds for obtaining various relative humidities are listed in Ref. 113). Similar techniques can be employed in the rehydration of freeze-dried films.

XIIB (2). Orientation of films

The measurement of infrared dichroic ratios for various absorption bands allows determination of the orientation of the chemical bonds involved in the absorbing mode. For optimal results, the film should be as monodomain crystalline as possible, so that the molecules have a constant direction over the whole absorbing area. As discussed below and in Ref. 4, useful information may be obtained even with some degrees of randomness in the film, for example, head group transitions vector orientations have been obtained by dichroic measurements on phosphatidylethanolamine films, even though the phospholipid distributes randomly about a direction normal to the film plane (and hence randomly about the polarization axis of any beam indirect normal to the plate).

Usual methods for orienting thin films involve the use of substrates that possess an orienting action on the film molecules. Suitable surfaces have been prepared by etching, rubbing or mechanically scribing of the substrate. These techniques for achieving alignment do not seem to yield very complete or stable orientation [98,114]. A new procedure [115], developed for orienting liquid-crystal electro-optical devices, may have wide usefulness in infrared film studies. The method achieves orientation by the use of surface coupling agents, molecules which contain a group capable of orienting the film along with a moiety which will form a polymerized monolayer bonded to the substrate surface. Alkoxysilanes of the general form $RSiX_3$ (where R is an orienting group attached to the silicon in a thermally and hydrolytically stable manner and X indicates alkoxyl groups) seem particularly useful. For example, Powers and Clark [115] have successfully produced thick (approx. 10^5 bilayers) monodomain films of phospholipid/water and phospholipid/water/cholesterol mixtures by slow annealing of the appropriate mixtures contained between glass slides coated with the silicone surfactant *N,N*-dimethyl-*N*-octadecyl-3-aminopropyltrimethoxysilyl chloride. The orientation of the phospholipid about an axis normal to the film surface remains random; however, surface-coupling agents could likely be used along with an etched substrate surface to achieve more complete alignment in a chosen direction parallel to the film plane.

Film samples may be carefully peeled from the orienting substrates for use in X-ray diffraction or infrared absorption studies. There are no coupling agents that will bond readily to the hydrophobic silver bromide window [116].

XIIB (3). Pressed halide disc techniques

In the case of solid samples that will not form films readily (such as ionic substances

that form discrete, large crystals on the plate surface) or in situations where random orientation is desired, compressed KBr pellets may be used for infrared analysis. This method of sample preparation, treated in most general references on infrared analytical techniques [117,118] involves grinding several milligrams of the sample in an agate mortar, mixing with finely powdered, anhydrous KBr and then subjecting the mixture to high pressure. Under pressure, the matrix material fuses to a transparent pellet which may be examined by standard infrared techniques. Hydraulic presses exist for pellet production but inexpensive hand-operated presses are satisfactory for occasional use.

It is particularly important when examining biological substances that possible effects of grinding the sample be considered. It is well-known that grinding of materials such as phospholipids that exist in several polymorphic forms may induce physical changes in the sample. In addition, special infrared quality KBr, which should be stored in a dessicator at 110°C to maintain dryness, is required for the matrix. Even so, the samples will likely contain a small amount of water. This water may affect the transparency of the pellet at low frequencies.

XIIB (4). Other sampling methods

Other sampling techniques that may be useful in infrared spectroscopy of biological systems include the production of oil mulls and a new procedure for incorporating bilayer arrays into a clay matrix material [105]. The use of oil mulls (which are simply dispersions of the sample in an infrared-transparent oil) is covered in Ref. 117. Mulls appear to have no particular values over KBr pellets for the study of membrane-related systems.

A newer preparative method that may have potential employs hectorite clay as a matrix material. This clay is a microcrystalline silicate with a large internal surface area (typically 800 m^2/g) and layered structure consisting of silicate sheets separated by layers of hydrated cations. Under the appropriate ionic conditions, the clay may be colloidally dispersed in water to expose the internal surface to an absorbant molecule. Subsequent drying on a plastic sheet allows the layered structure to reform and the absorbate may be incorporated into the interlayer regions in a structured manner. The resulting thin (approx. 25 μm) transparent discs may be removed from their drying surfaces, examined spectroscopically and even stored. The gel liquid-crystal transition as indicated by CH-stretching ratios occurs at about 40°C for dipalmitoyl phosphatidylcholine liposomes thus prepared in hectorite, suggesting that the lipid bilayer structure is preserved by the silicate matrix. Unfortunately, the clay has strong absorptions below 1100 cm^{-1}, which prevents access to the low frequency spectrum.

XIIC. Experimental procedures and methods of analysis

XIIC (1). Temperature control

As infrared spectroscopy necessarily involves the absorption of energy and attendant heating of material in the beam, temperature control of the sample is an important consideration in the spectroscopy of thermally-sensitive biomaterials. This is of course particularly true when temperature-structure studies are intended.

As indicated above, AgBr is an effective electrical and thermal insulator. It is thus essential that the heat exchanger used for temperature control contacts as much of the plate area as possible, without blocking the beam path. Temperature control by a flow of constant temperature gas flow (dry N_2) around the sample would appear preferable.

however, we know of no such systems. We have routinely employed a solid aluminum block (5 X 12 X 3 cm), thermally insulated from the spectrometer, as a sample holder. The temperature of the block is maintained by a circulating liquid coolant pumped from a constant temperature bath through channels bored into the holder. We monitor the sample temperature with a small thermistor attached to the AgBr window, but shielded from direct source radiation.

The newest generation of commercial infrared spectrometers (e.g. Perkin-Elmer models 580, 180) employ dual chopping systems that expose the sample to the infrared source for only one-quarter of the time. The problem of sample heating in such cases is, of course, considerably reduced. In situations involving critical temperature control (as in phase-transition studies), the advantages of dual chopping are likely significant.

XIIC (2). Compensation for solvent absorptions

As already noted the application of infrared absorption techniques to biological systems is hindered by the intense absorption of water throughout the fundamental region. Since double-beam spectrometers record the difference between sample and reference absorptions, it is possible in such systems to remove the effects of water absorption by measuring the [sample and solvents] vs. [solvent alone] spectrum. The reference cell is typically a variable pathlength liquid cell, whose thickness is adjusted to give equivalent solvent absorption in the two beams. However, when using this technique in regions of high solvent absorption, there will be little power available at the infrared detector. Optical null spectrometers may then still provide inaccurate data in these regions. Spectrometers using electronic ratioing have a 'live zero' and are thus immune to this type of signal distortion [117]. (See Section IIIA for this technique applied to phospholipid/water mixture.)

XIIC (3). Measurements of infrared dichroic ratios

A useful application of infrared analysis involves the determination of molecular conformations by the measurement of infrared dichroic ratios, i.e. the ratios of sample absorbance for two orthogonal polarizations of the incident radiation. Because of the potential of this technique, we consider the method in some detail.

A particular vibrational mode absorbs infrared radiation if the molecular motion produces a fluctuating dipole moment. This transition moment is a vector quantity which has a defined direction with respect to the bonds involved. The transition moment is approximately parallel (perpendicular) to the bond orientation for pure stretching (bending) modes; mixed vibrations, such as the peptide amide absorptions, show intermediate alignment [119]. Since the oscillating dipole only absorbs the component of the incident radiation parallel to its transition moment, measurement of the sample absorbance for two perpendicular polarizations allows deduction of the orientation of the transition moment with respect to the spectrometer. Thus in simple cases, dichroic ratios yield direct information about the molecular conformation. There are many general references to polarized infrared spectroscopy [119]; we wish to discuss particulars involved in obtaining dichroic data on film samples, as these are most likely to be of use in membrane-related studies. The success of dichroic measurements clearly depends on the degree of sample order. Only if a given transition moment has a constant orientation over the whole sample will results be optimal. However, as Akutsu et al. indicate [99], there are many situations in which partially-ordered systems may also provide some useful polarization data.

Ref. 99 first considers molecular films in which a transition vector of interest distributes uniformly about the z-axis, taken as the propagation direction of the incident radiation. Although the transition vectors have a fixed angle θ with respect to the z-axis, the absorbances A_x and A_y for x and y incident polarizations are equal, since the molecules have no prefered direction in the film (y–y) plane. This situation is typical for example, of head group bonds of multibilayer phospholipid films. The dichroic ratio $R_{xy} = A_y/A_x$ is thus unity.

If the film is rotated by an angle about the x-axis, so that the z-axis (the xyz coordinates are fixed with respect to the film plane) makes an angle α, with the z'-axis, which now lies along the propagation direction of the incident radiation, one has the following absorbances $A_{x'}$ and $A_{y'}$ obtained by simple transformation of coordinates.

$$A_x^{1'} = AM^2 \sin^2\theta \tag{1}$$

$$A_y^{1'} = AM^2 (\cos^2\alpha \sin^2\theta + 2 \sin^2\alpha \cos^2\theta) \tag{2}$$

in which AM^2 is constant, related to the film thickness and the magnitude of the transition moment and α is the angle of the incident radiation in the films, given in terms of α_0 and the refractive index n, of the film by Snell's law:

$$n \sin\alpha = \sin\alpha_0 \tag{3}$$

By combining Eqns. 1–3 the dichroic ratio $R_{y'x'}$ is shown to be

$$R_{y'x'} = 1 + \frac{1}{n^2} \sin^2\alpha_0 (2 \cot^2\theta - 1) \tag{4}$$

A measurement of $R_{y'x'}$ with film plane rotated a known angle α_0 with respect to normal orientation, along with knowledge of n thus gives θ, the transition moment angle with the z-axis.

Akutsu et al. [99] also consider the more complex situation, in which the molecules distribute randomly about the z-axis, normal to the film plane and in addition part of the molecule distributes uniformly about a second rotation axis that is tilted at an angle γ with respect to the z-axis. Hydrocarbon chains in lipid multilayers may well be arranged in such a manner [99]. In this case, analysis similar to the above gives $R_{y'x'}$ for the film of refractive index n rotated through an angle α_0 about the x-axis as

$$R_{y'x'} = \frac{2 - (2/n^2) \sin^2\alpha_0 + ({}^3/n^2 \sin^2\alpha_0 - 1) \sin^2\gamma}{2 - \sin^2\gamma} \tag{5}$$

As before, measurement of $R_{y'x'}$ allows determination of γ, the orientation angle of the second rotation axis. Use of these methods to deduce the head group conformation of built-up films of phosphatidylethanolamine is discussed in Section IIIA (1).

XIIC (4). Modulated-excitation infrared spectroscopy

As a final example of the specialized infrared techniques that may be valuable to membrane studies, we mention the use of modulated excitation infrared spectroscopy as applied by Fringeli and Gunthard [103] to obtain data on the hydration sites of egg phosphatidylcholine. The method is a type of discriminating spectroscopy in which the intensity of an absorption band is modulated periodically by some external reaction and the resulting signal is synchronously detected, thus yielding vastly increased sensitivity against those absorption bands unaffected by the modulating reaction. As with all

methods involving synchronous detection, kinetic information is available through measurement of the frequency dependence of the intensity and phase angle (between stimulation and response) of the detected signal. Bands in modulated excitation are of two types. Type 1 bands are due to the specific absorptions of the modulating substance (if any) and have the typical appearance of absorption bands. Type 2 bands result from the induced changes in the system and are generally biphasic, since they arise from superposition of decreasing and increasing absorption bands at nearby frequencies. For example, hydration of an ester shifts the $\nu c = o$ absorption to lower wavenumbers; thus if an ester group be hydrated, absorption increases at the lower wavenumber and correspondingly decreases at the position of the anhydrous vibration (since the amount of unhydrated C=O becomes less). Therefore, conformational and direct changes in the spectra are separable. Thus, Fringeli and Gunthard [103] modulate the hydration of phosphatidylcholine films at a rate of 1.5 Hz by periodic injection of wet (90% rh) N_2 into a stream of drier N_2 (60% rh) that constantly flushes the sample. In order to achieve a reasonable response at this frequency, very thin (4–6 bilayers) films were employed. These were examined by attenuated total reflectance spectroscopy to obtain sufficient absorption.

XIII. Results

We conclude with a survey of the specific results obtained thus far on membrane-related systems by means of the techniques outlined in Section II. We discuss separately work in phospholipids, which has proceeded well in both theoretical and experimental areas, and peptide research, which is primarily theoretical.

XIIIA. Phospholipids

The infrared literature on phospholipids addresses significant research in the areas of head group and acyl chain vibrations. Preliminary absorption spectra of films of phosphatidylcholine [120] and phosphatidylethanolamine [121] obtained by Chapman and coworkers, allowed identification of the primary CH-stretching and bending modes, the carbonyl absorption, the OH-stretching and bending bands in hydrated samples and the complex phosphate vibrations. These early results showed that the phospholipid spectra, particularly below 1400 cm^{-1}, were extremely variable, changing markedly with temperature and method of sample preparation. Spectra of cold or anhydrous films exhibited considerable fine structure which vanished on bringing to room temperature or hydration.

These results were extended by us [97] when we studied multibilayer films of phosphatidylcholine, phosphatidylethanolamine and mixed films of phosphatidylcholine/phosphatidylethanolamine (1 : 1, mol/mol) as a function of fatty acid composition, temperature, and hydration in order to clarify band assignments and examine the head group interactions among the different phosphatides. Fig. 16 compares spectra in the range 700–850 cm^{-1} and 1200–3600 cm^{-1} of dipalmitoyl phosphatidylcholine (anhydrous and monohydrate) and anhydrous dipalmitoyl phosphatidylethanolamine (evaporated from both chloroform and chloroform/methanol, 2 : 1, v/v) and shows the principal difference between the various systems. Table II lists the corresponding band assignments. We interpret the lowered phosphoryl absorption in the phosphatidylethanolamine spectra as due to $NH \rightarrow O$ hydrogen bonding of the ethanolamine head group, which can align tangentially to the bilayer plane, permitting closer packing of the mole-

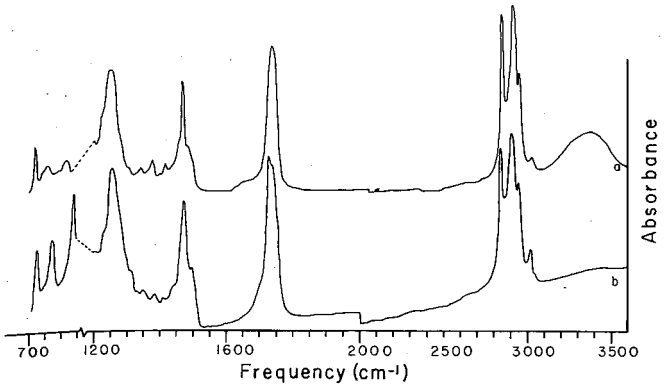

Fig. 16. Infrared absorption spectra (at 20°C) from 700–850 and 1200–3600 cm^{-1} of multibilayers of (a) dipalmitoyl phosphatidylcholine monohydrate, and (b) anhydrous dipalmitoyl phosphatidylcholine. From Ref. 97 with kind permission from Academic Press, New York.

TABLE II

INFRARED-ACTIVE BANDS (IN cm^{-1}) OF VARIOUS PHOSPHATIDYLCHOLINES (PC) AND PHOSPHATIDYLETHANOLAMINES (PE)

All films were prepared from solutions in chloroform/methanol (2 : 1, v/v), except for dipalmitoyl phosphatidylethanolamine films which were prepared from a chloroform solution. Abbreviations: DPPC = dipalmitoyl phosphatidylcholine, DLPC = dilauroyl phosphatidylcholine, DPPE = dipalmitoyl phosphatidylethanolamine, s = shoulder.

Band	DPPC (dry)	DPPC (mono-hydrate)	DLPC (dry)	Egg PC (dry)	DPPE (dry)	DPPE (mono-hydrate)	Egg PE (dry)
$\nu_s CH_2$	2848	2849	2848	2853	2848	2848	2848
$\nu_{as} CH_2$	2915	2918	2915	2920	2918	2915	2918
$\nu_{as} CH_3$	2957	2958	2953	2959	2958	2956	2958
δCH_2	1461	1466	1467	1469	1462	1469	1462
					1471		
ν(G=O)	1724	1733	1734	1740	1739	1720	1740
	1734					1730	
ν(P=O)	1254	1248	1252	1260	1222	1215	1224
					1241 s		1240 s
terminal CH_2 rock	722	721	720	720	715	720	720
					725		
$\nu(CH_2)$ of N^+CH_3	3028	3028	3028	3013			
$\nu(NH_3^+)$ *					2128	2108	2558
					2328	2328	2638
					2558	2548	2708
					2646		
					2688		
					2728	2728	
$\delta(NH_3^+)$					1550	1580	1559
					1625	1620	1638
ν(OH)		3373					
δ(OH)		1645					

* The ionized, hydrogen-bonded NH_3^+ group displays multiple weak band progressions in the range of 2000–2700 cm^{-1}.

cules than is possible in phosphatidylcholine. The closer packing results in strong crystal field effects which produce the complex fine structure revealed in the phosphatidylethanolamine spectra. Splitting of the CH-bending fundamental at about 1460 cm^{-1} and the terminal CH_2 rocking mode at about 720 cm^{-1} reveal further that the acyl chains of the phosphatidylethanolamine film are packed in orthorhombic rather than hexagonal arrays. The lack of fine structure on monohydration of phosphatidylcholine is also attributed to the decreased intermolecular (crystal field) interactions that occur as water is inserted into the head group lattice, increasing the intermolecular separations. The absence of further change upon complete hydration suggests that only the initial water bonds tightly to the phosphatide.

Spectra in the low frequency region (300–800 cm^{-1}), shown in Fig. 17, shows these changes most sensitively. Detailed assignments in this complex and variable parts of the spectrum, which will require dichroic experiments on well-oriented films and work with deuterated or ^{13}C-labeled phospholipid analogues is essential to future progress in this area. Such research, likely involving analysis of the collective modes of the head group lattice, is crucial.

Our recent work [97] also deals with the vibrations of the phosphate stretching region about 800–1200 cm^{-1}. The difference here, shown in Fig. 18, appears between pure phosphatidylethanolamine films and those of either pure phosphatidylcholine or mixed phosphatidylethanolamine-phosphatidylcholine systems. We interpret the two classes of

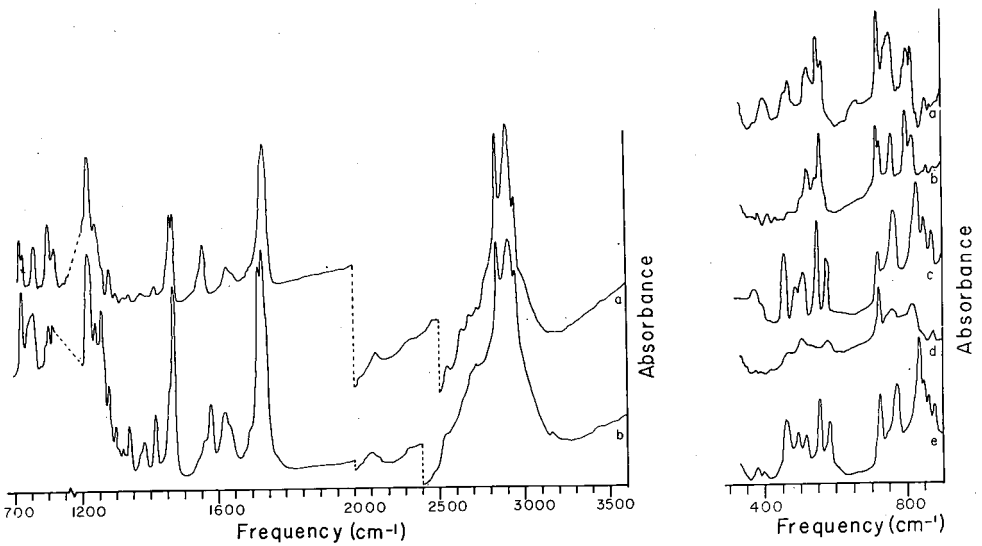

Fig. 17. Infrared absorption spectra from 700–850 and 1200–3600 cm^{-1} of multibilayers of anhydrous dipalmitoyl phosphatidylethanolamine evaporated from solution in (a) chloroform/methanol (2 : 1, v/v), and (b) chloroform. From Ref. 97, with kind permission of Academic Press, New York.

Fig. 18. Infrared absorption spectra (at 20°C) from 300–800 cm^{-1} (low frequency region) of multibilayers of: (a) dipalmitoyl phosphatidylethanolamine prepared from chloroform solution; (b) dipalmitoyl phosphatidylethanolamine from chloroform/methanol (2 : 1, v/v); (c) anhydrous dilauroyl phosphatidylcholine; (d) dipalmitoyl phosphatidylcholine monohydrate; and (e) anhydrous dipalmitoyl phosphatidylcholine. From Ref. 97, with kind permission from Academic Press, New York.

spectra (a doublet at about 1085 and 1055 cm^{-1}, with secondary absorption at about 968 cm^{-1} vs. individual strong bands at around 1080 and 1010 cm^{-1}) as arising from head group orientation tangential vs. normal to the bilayer plane. These changes arise because the absorptions in this region are due to the P-O-C aliphatic linkage which always occurs in pairs that share a phosphorus atom (resulting in coupled modes) and because the relative orientation of the two attendant P-O-C transition moments varies greatly as the head group moves from a tangential to a perpendicular conformation with respect to the film plane. We note that hydration isotherm measurements [112] suggest similar structural details of pure and mixed systems to those we postulate.

A somewhat surprising finding of this research was that mixtures of phosphatidylcholine and phosphatidylethanolamine will not form a mixed phase at neutral pH. It appears that the hydrogen-bonded phosphatidylethanolamine structure is so energetically favorable that the entropic advantage of a mixed phase (which would require disruption of the NH → O hydrogen bonds and a normal conformation of the phosphatidylethanolamine head group) is insufficient to allow intermixing of the two phospholipid classes. Mixing occurs readily, however, when the amino group charge is neutralized by the OH^- (pH 11). Uniphase mixtures of egg phosphatidylcholine/phosphatidylethanolamine form easily, even at pH 7.0, presumably because the unsaturated acyl chains cannot pack sufficiently tightly to allow energetic (short) NH → O hydrogen-bonding.

XIIIA (1). Infrared dichroic measurements on dipalmitoyl phosphatidylethanolamine multilayers

More specific conformational details of phosphatide multibilayers have been deduced by Akutsu et al. [99], who used the techniques outlined in Section IIC (3) to obtain the directions for selected transition moments in built-up films of dipalmitoyl phosphatidylethanolamine. These workers evaluated dichroic ratios for six vibrational modes: CH_2 symmetric and asymmetric stretching, CH_2 scissoring, C=O stretching, PO_2^- asymmetric stretching and C–C–N^+ asymmetric stretching. In all cases, no dichroism in the x-y plane could be observed for incident radiation in the Z-direction, normal to the multilayer plane. This indicates that the molecules distribute randomly about the z-axis. When the film plane was rotated about the x-axis by $\alpha_0 = 30^\circ$ (in some cases, independent measurements were done at $\alpha_0 = 45^\circ$ to check for consistency of the method) dichroism in the x'-y' plane appeared, as described in Section IIC (3). From the measured dichroic ratios, the authors calculated the transition vector orientations shown in Table III. They found that the moments of C=O stretching, and the PO_2^- and C–C–N^+ asymmetric stretching modes orient nearly parallel to each other and deviate by less than 20° from the film plane. They also found that the hydrocarbon chain axes are tilted at about 75° to the film plane. These results, demonstrating that the phosphatidylethanolamine film is very tightly packed with the hydrogen-bonded polar moiety alligned along the film surface, are in accord with our results [97].

XIIIA (2). Phospholipid acyl chain results

The symmetric and asymmetric CH_2- and CH_3-stretching vibrations of acyl chains are predominant features of both the Raman and infrared spectra of phospholipids. However, the infrared spectra fail to show the dramatic changes with temperature that characterize the Raman bands. Asher and Levin [100] have investigated in detail the behavior of the infrared CH-stretching vibrations of multilamellar liposomes and single-shell vesicles of dipalmitoyl phosphatidylcholine/water dispersions throughout the gel ⇌ liquid crystal

TABLE III

ORIENTATION OF TRANSITION MOMENTS (γ^0) IN HYDROCARBON CHAIN

Wavenumber (cm^{-1})	Assignment	Transition moment	pH 2.6 ($\alpha_0 = 30°$)	pH 6.8 ($\alpha_0 = 30°$)	pH 6.8 ($\alpha_0 = 45°$)
2918	CH_2 antistretch		16^{+6}_{-11}	12^{+9}_{-12}	10^{+4}_{-10}
2852	CH_2 symmetric stretch	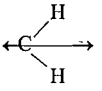	12^{+9}_{-12}	11^{+8}_{-11}	8^{+5}_{-8}
1467	CH_2 scissoring	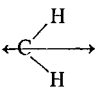	11^{+16}_{-11}	15^{+13}_{-15}	

phase transition. They find that the phase transition produces distinct changes in the frequencies of the CH_2 symmetric and asymmetric band maxima without significant shifts in their relative intensities. In pure phosphatidylcholine multilayers, the asymmetric CH_2-stretching maximum shifts from 2920 to 2924 cm^{-1} abruptly at 41°C (transition width about 2°C). The symmetric mode shows a smaller but distinct shift of 2.5 cm^{-1} (2853.0 to 2855.5 cm^{-1}) at the same temperature. Their data for both multilayers and vesicles are shown in Figs. 20 and 21. It is significant that the phase transition temperature as determined by this work is in good agreement with that found by other methods.

The authors have extended their work to more complex systems, using the CH_2 frequency shift to monitor phase transitions in dipalmitoyl phosphatidylcholine/

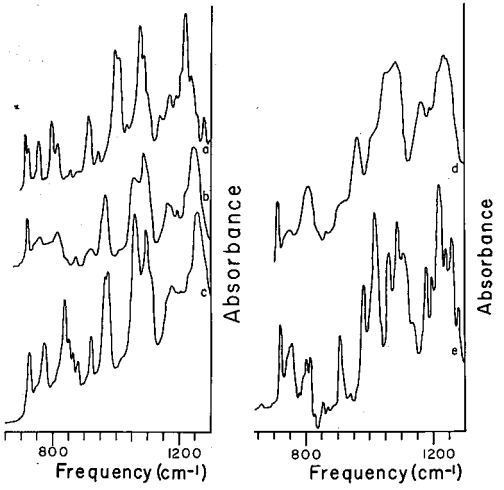

Fig. 19. Infrared absorption spectra from 800–1200 cm^{-1} (phosphate region) of multibilayers of: (a) dipalmitoyl phosphatidylethanolamine evaporated from chloroform/methanol (2 : 1, v/v); (b) dipalmitoyl phosphatidylcholine monohydrate; (c) anhydrous dipalmitoyl phosphatidylcholine; (d) equimolar dipalmitoyl phosphatidylcholine and dipalmitoyl phosphatidylethanolamine at pH 7.0; and (e) dipalmitoyl phosphatidylethanolamine evaporated from chloroform. From Ref. 97, with kind permission of Academic Press, New York.

cholesterol/water and dipalmitoyl phosphatidylcholine/cholesterol/amphotericin B vesicles. The results, showing broadening of the transition, are in accord with Raman studies.

An important feature of the above work is the use of compensated spectra. The samples were held in a variable temperature Irtan-2 cell (path length 27 μm) and a matching cell, containing only water, was placed in the reference beam. In this way, spectra could be recorded despite the 80% water content of the lipid dispersions.

In a careful theoretical study of the vibrational spectra of the polymethylene chain in the CH-stretching region, Snyder et al. [41] discuss the vastly different sensitivities of the Raman and infrared bands to molecular conformation and environment. Essentially, the complexities in the CH stretching region in both the Raman and infrared involve Fermi-resonance between the symmetric CH_2 stretching mode and a binary continuum of methylene bending states, as described in Section IIIA (1). However, because of symmetry considerations, different combinations of states are involved in the absorption and scattering spectra. The broad secondary maxima that complicate the CH stretching region are centered near extrema of the appropriate binary dispersion curve, since the density of binary states is largest there; the intensity of these secondary bands is proportional to the separation between the binary states and the CH-stretching fundamental. Thus, in the infrared, critical points of the appropriate binary dispersion occur at 2921 and 2910 cm^{-1} resulting in broad bands centered at 2922 and 2898 cm^{-1}. These frequen-

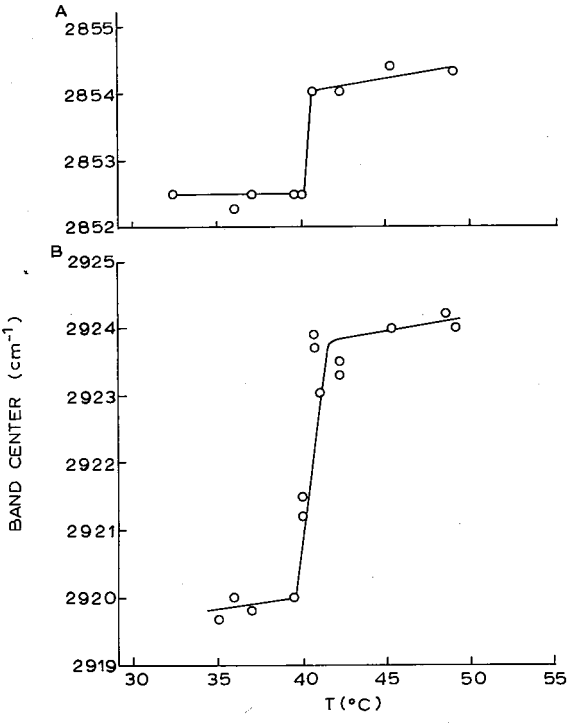

Fig. 20. Temperature profile for dipalmitoyl phosphatidylcholine/water multilayers using the frequency shifts for the symmetric methylene stretching mode (A), and the asymmetric methylene stretching mode (B). From Ref. 100.

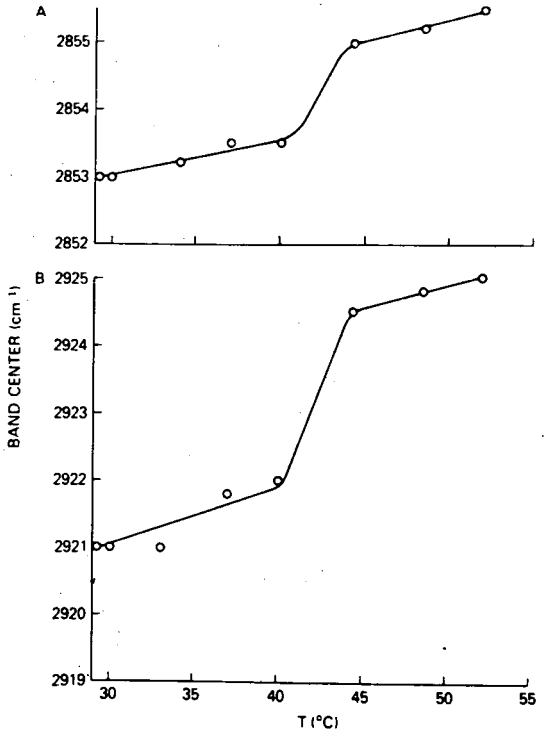

Fig. 21. Temperature profile for dipalmitoyl phosphatidylcholine/water vesicles using the frequency shifts for the symmetric methylene stretching mode (A), and the asymmetric methylene stretching mode (B). From Ref. 100.

cies are quite remote from the CH symmetric stretch at 2855 cm^{-1}; thus the bands are weak and mostly obscured by the strong CH asymmetric stretch at 2920 cm^{-1}.

We mention that studies of this nature are of prime importance to the development of infrared (and Raman) techniques for membrane biology, since the subtle conformationally sensitive aspects of the spectra often depend on resonance or crystalline field effects.

XIIIA (3). Hydration of egg phosphatidylcholine

As a final example of phospholipid research, we indicate the use of modulated excitation (Section IIC (4)) to determine hydration sites of egg phosphatidylcholine [122]. These authors find type 1 bands (terminology of Section IIC (4)) at 3360 and 160 cm^{-1} clearly due to OH-stretching and bending of water molecules. From other bands in the spectrum, they conclude that hydration sites are the PO_2^- group, the C=O group and possibly the choline group. No bands in the modulated excitation spectrum occurred in the CH-stretching or bending region, indicating that the acyl chains are not affected by the hydration process.

XIIIB. Polypeptides

Extensive literature exists on the infrared spectra of polypeptides; however, there has been little application to membrane-related systems. It has long been known that the

complex vibrations of the amide group (the amide I-V and amide A, B bands) change greatly with the local environment in polypeptides and are thus extremely sensitive to both the backbone conformation and the orientation of acyl side chains. In addition, the behavior of low frequency collective modes conveys much information since these vibrations reflect the global state of the polypeptide.

Some simple correlations exist. For example, the amide I band is near 1652 cm^{-1} in α-helical protein and close to 1625 cm^{-1} in β-structures [96]. Antiparallel β-conformations also show a shoulder at 1693 cm^{-1} [96]. These correlations have been used by Graham and Wallach [111] to observe changes in the conformation of mitochondrial membrane protein when the membranes are quick-frozen (see Section IIB (1) in various respiratory states. Electron transport increases antiparallel β-structure, which is reversed by inhibiting respiration or inducing phosphorylation with ADP.

Theoretical progress in the normal modes of polypeptides is crucial to development of conformationally sensitive methods of analysis. This work is proceeding systematically. Thus Moore and Krimm [101,102] have refined successively more useful valence force fields for polypeptides by beginning with a treatment of *N*-methylacetamide, then examining nylons and some deuterated derivatives [123] and finally studying polyglycine, β-poly(L-alanine) and β-poly(L-analylglycine). The final results are quite general, including transition dipole coupling and hydrogen bonding terms which are necessary to explain the splitting of the amide I and II bands. Agreement with published infrared and Raman data for these polypeptides is excellent and the derived force field is transferable to related systems, demonstrating that the theoretical approach is sound.

It is likely that as infrared data on freeze-dried membrane components and reconstituted model systems become available, the application of this theory to structural (functional) conformational changes in biomembranes will be valuable.

References

1 Colthup, N.B., Daly, L.H. and Wiberly, S.E. (1975) Introduction to Infrared and Raman Spectroscopy pp. 324–325, Academic Press, New York, NY
2 Wallach, D.F.H. and Winzler, R.J. (1974) Evolving Strategies and Tactics in Membrane Research Chapter 4, pp. 140–189, Springer-Verlag, New York, NY
3 Larsson, K. and Rand, R.P. (1973) Biochim. Biophys. Acta 326, 245–255
4 Mendelsohn, R., Sunder, S. and Bernstein, H.J. (1976) Biochim. Biophys. Acta. 443, 613–617
5 Verma, S.P. and Wallach, D.F.H. (1977) Biochim. Biophys. Acta 486, 217–227
6 Lippert, J.L. and Peticolas, W.L. (1971) Proc. Natl. Acad. Sci. U.S. 68, 1572–1576
7 Lippert, J.L. and Peticolas, W.L. (1972) Biochim. Biophys. Acta 282, 8–17
8 Mendelsohn, R. (1972) Biochim. Biophys. Acta 290, 15–21
9 Bulkin, B.J. and Krishnamachari, N. (1972) J. Am. Chem. Soc. 94, 1109–1112
10 Lis, L.J., Kauffman, J.W. and Shriver, D.F. (1975) Biochim. Biophys. Acta 406, 453–464
11 Spiker, R.C. and Levin, I.W. (1975) Biochim. Biophys. Acta 388, 361–373
12 Verma, S.P. and Wallach, D.F.H. (1975) Biochim. Biophys. Acta 401, 168–176
13 Mendelsohn, R., Sunder, S. and Bernstein, H.J. (1975) Biochim. Biophys. Acta 413, 329–340
14 Mendelsohn, R., Sunder, S. and Bernstein, H.J. (1976) Biochim. Biophys. Acta 419, 563–569
15 Gaber, B. and Peticolas, W.L. (1977) Biochim. Biophys. Acta 465, 260–274
16 Yellin, N. and Levin, I.W. (1977) Biochemistry 16, 643–647
17 Yellin, N. and Levin, I.W. (1977) Biochim. Biophys. Acta 468, 490–494
18 Lis, L.J., Kauffman, J.W. and Shriver, D.F. (1976) Biochim. Biophys. Acta 436, 513–522
19 Lis, L.J., Goheen, S.C., Kauffman, J.W. and Shriver, D.F. (1976) Biochim. Biophys. Acta 443, 331–338
20 Verma, S.P. and Wallach, D.F.H. (1976) Biochim. Biophys. Acta 426, 616–623

21 Weidekamm, E., Bamberg, E., Brdiczka, D., Wildermuth, G., Macco, F., Lehmann, W. and Weber, R. (1977) Biochim. Biophys. Acta 464, 442–447
22 Curatolo, W., Verma, S.P., Sakura, J.D., Small, D.M., Shipley, G.G. and Wallach, D.F.H. (1978) Biochemistry 17, 1802–1807
23 Lippert, J.L., Gorczyca, L.E., Meiklejohn, G. (1975) Biochim. Biophys. Acta 382, 51–57
24 Wallach, D.F.H. and Verma, S.P. (1975) Biochim. Biophys. Acta 382, 542–551
25 Verma, S.P., Wallach, D.F.H. and Schmidt-Ullrich, R. (1975) Biochim. Biophys. Acta 394, 633–645
26 Schmidt-Ullrich, R., Verma, S.P. and Wallach, D.F.H. (1976) Biochim. Biophys. Acta 426, 477–488
27 Verma, S.P. and Wallach, D.F.H. (1976) Biochim. Biophys. Acta 436, 307–318
28 Verma, S.P. and Wallach, D.F.H. (1976) Proc. Natl. Acad. Sci. U.S. 73, 3558–3561
29 Verma, S.P., Schmidt-Ullrich, R., Thompson, W.S. and Wallach, D.F.H. (1977) Cancer Res. 37, 3490–3493
30 Milanovitch, F.P., Shore, B. and Harney, R.C. (1976) Chem. Phys. Lipids 17, 79–84
31 Milanovitch, F.P., Yeh, Y., Baskin, R.J. and Harney, R.C. (1976) Biochim. Biophys. Acta 419, 243–250
32 Rothschild, K.J., Andrew, J.R., deGrip, W.J. and Stanley, H.E. (1976) Science 191, 1176–1178
33 Bunow, M.W. and Levin, I.W. (1977) Biochim. Biophys. Acta 464, 202–216
34 Schmidt-Ullrich, R., Verma, S.P. and Wallach, D.F.H. (1975) Biochem. Biophys. Res. Commun. 67, 1062–1069
35 Chen, M.C. and Lord, R.C. (1976) Biochemistry 15, 1889–1897
36 Landon, D.O. and Reed, P.R. (1972) Spex. Speaker 17, 4–12
37 Genzel, L., Keilmann, F., Martin, T.P., Winterling, G., Yacoby, Y., Frölich, H. and Makinen, M.W. (1976) Biopolymers 15, 219–225
38 Yacoby, Y. and Linz, A. (1974) Phys. Rev. B9, 23–24
39 Bridoux, M. and Delhaye, M. (1970) Nouv. Rev. Opt. Appl. 1, 23–24
40 Schachtschneider, I. and Snyder, F. (1963) J. Polym. Sci. C7, 99–122
41 Snyder, R.G., Hsu, F.L. and Krimm, S. (1978) Spectrochim. Acta, Part A 34. 395–406
42 Verma, S.P. and Wallach, D.F.H. (1977) Biochem. Biophys. Res. Commun. 74, 473–479
43 Brandts, J.F. and Hunt, L. (1967) J. Am. Chem. Soc. 89, 4826–4838
44 Karvaly, B. and Loshchilova, E. (1977) Biochim. Biophys. Acta 470, 492–496
45 Eisenberg, D. and Kauzmann, W. (1969) The Structure and Properties of Water, pp. 121–135, Oxford University Press, Oxford
46 Eisenberg, D. and Kauzmann, W. (1969) The Structure and Properties of Water, pp. 228–246, Oxford University Press, Oxford
47 Mizushima, S. and Shimanouchi, T. (1949) J. Am. Chem. Soc. 71, 1320–1324
48 Shaufele, R.F. and Shimanouchi, T. (1967) J. Chem. Phys. 47, 3605–4175
49 Shimanouchi, T. (1973) Pure Appl. Chem. 33, 93–107
50 Brown, K.G., Erfurth, S.L., Small, W.W. and Peticolas, W. (1972) Proc. Natl. Acad. Sci. U.S. 69, 1467–1469
51 Takeuchi, H., Shimanouchi, T., Tasumi, M., Vergoten, G. and Fleury, G. (1974) Chem. Phys. Lett. 28, 449–451
52 Peticolas, W.L., Hibler, G.W., Lippert, J.L., Peterlin, A. and Olf, H. (1971) Appl. Phys. Lett. 18, 87–90
53 Fanconi, B. and Peticolas, W.L. (1971) Biopolymers 10, 2223–2229
54 Amer, N.M. and Shen, Y.R. (1973) Solid State Commun. 12, 263–265
55 Lippert, J.L. and Peticolas, W.L. (1972) Biochim. Biophys. Acta 282, 8–17
56 Gaber, B.P., Yager, P. and Peticolas, W.L. (1978) Biophys. J. 21, 161–176
57 Chrisman, R., English, J.C. and Tobias, R.S. (1976) Appl. Spectrosc. 30, 168–179
58 Larsson, J. (1973) Chem. Phys. Lipids 10, 165–180
59 Faiman, R. (1977) Chem. Phys. Lipids. 18, 84–104
60 Hinz, H.J. and Sturtevant, J.M. (1972) J. Biol. Chem. 247, 3697–3700
61 Amati, D. and Lago, C. (1975) Cold Spring Harbor Symp. Quant. Biol. 39, 371–374
62 Lago, C., Sartorius, B., Tarmontano, D. and Amati, D. (1977) J. Cell Physiol. 92, 265–274
63 Mendelsohn, R. and Maisano, J. (1978) Biochim. Biophys. Acta 506, 192–201
64 Mabrey, S. and Sturtevant, J.M. (1977) Biochim. Biophys. Acta 486, 444–450
65 Finkelstein, A. and Cass, A. (1968) J. Gen. Physiol. 52, 145S

66 Szabo, G., Eisenman, G., Laprade, R., Ciani, S.M. and Krasne, S. (1973) in Membranes Vol.2 (Eisenman, G., ed.), pp. 179–328 Dekker, New York, NY
67 Rosenberg, B. and Jendrasiak, G.L. (1968) Chem. Phys. Lipids 2, 47–54
68 Loshchilova, E. and Karvaly, B. (1977) Chem. Phys. Lipids 19, 159–168
69 Weidekamm, E., Bamberg, E., Brdiczka, D., Wildermuth, G., Macco, F., Lehmann, W. and Weber, R. (1977) Biochim. Biophys. Acta 464, 442–447
70 Racker, E. and Eytan, E. (1975) J. Biol. Chem. 250, 7533–7544
71 Racker, E. (1976) J. Cell Physiol. 89, 697–700
72 Racker, E. (1975) Biochem. Soc. Trans. 3, 785–802
73 Shamoo, A.E. and Ryan, T.E. (1975) Ann. N.Y. Acad. Sci. 264, 83–97
74 Racker, E. and Fischer, L.W. (1975) Biochem. Biophys. Res. Commun. 67, 1144–1150
75 Folch-Pi, J. and Sakura, J.D. (1976) Biochim. Biophys. Acta 427, 410–427
76 Pinto da Silva, P. and Miller, R.G. (1975) Proc. Natl. Acad. Sci. U.S. 72, 4046–4050
77 Bogg, J.M., Vail, W.J. and Moscarello, M.A. (1976) Biochim. Biophys. Acta 448, 517–530
78 Curatolo, W., Sakura, J.D., Small, D.M. and Shipley, G.G. (1977) Biochemistry 16, 2313–2319
79 Wallach, D.F.H. and Gordon, A.S. (1968) Fed. Proc. 27, 1263–1268
80 Marcelja, S. (1976) Biochim. Biophys. Acta 455, 1–8
81 Lippert, J.L., Tyminski, V. and Desmeules, J. (1975) J. Am. Chem. Soc. 98, 7075–7080
82 Koenig, J.L. (1972) J. Polymer Sci. 11, 2502–2520
83 Goheen, S.C., Gilman, T.H., Kauffman, J.W. and Garvin, J.E. (1977) Biochem. Biophys. Res. Commun. 79, 805–814
84 Bieri, V. and Wallach, D.F.H. (1975) Biochim. Biophys. Acta 406, 415–423
85 Ladbrooke, B.D. and Chapman, D. (1969) Chem. Phys. Lipids 3, 304–367
86 Gottlieb, M.H. and Eanes, E.D. (1974) Biochim. Biophys. Acta 373, 519–522
87 Peters, R., Peters, J., Tews, K.H. and Bahr, W. (1974) Biochim. Biophys. Acta 367, 282–294
88 Wallach, D.F.H., Verma, S.P., Weidekamm, E. and Bieri, V. (1974) Biochim. Biophys. Acta 356, 68–71
89 Verma, S.P. and Wallach, D.F.H. (1975) Biochim. Biophys. Acta 382, 73–82
90 Jackson, W.M., Kostyla, J., Nordin, J.H. and Brandts, J.F. (1973) Biochemistry 12, 3662–3667
91 Zimmer, G. and Schirmer, H. (1974) Biochim. Biophys. Acta 345, 314–320
92 Zimmer, G., Schirmer, H. and Bastian, P. (1975) Biochim. Biophys. Acta 401, 244–255
93 Lacko, L., Wittke, B. and Geck, P. (1973) J. Cell Physiol. 82, 213–218
94 Sato, B., Nishikida, K., Samuels, L.T. and Tyler, F.H. (1978) J. Clin. Invest. 61, 251–259
95 Hui, S.W. and Strozewski, C.M. (1978) Biophys. Soc. (Abstr.) 21, 37a
96 Wallach, D.F.H. (1975) Chem. Phys. Lipids 8, 347–354
97 Fookson, J.E. and Wallach, D.F.H. (1978) Arch. Biochem. Biophys. 189, 195–204
98 Verma, S.P., Wallach, D.F.H. and Smith, I.C.P. (1974) Biochim. Biophys. Acta 345, 129–140
99 Akutsu, H., Kyogoku, Y., Nakahara, H. and Fukuda, K. (1975) Chem. Phys. Lipids 15, 222–242
100 Asher, I.M. and Levin, I.W. (1977) Biochim. Biophys. Acta 468, 63–72
101 Moore, W.H. and Krimm, S. (1976) Biopolymers 15, 2439–2464
102 Moore, W.H. and Krimm, S. (1976) Biopolymers 15, 2465–2483
103 Fringeli, V.P. and Gunthard, H.H. (1976) Biochim. Biophys. Acta 450, 101–106
104 Air Dryers, Perkin-Elmer Accessory Data Sheet L-81, Perkin-Elmer Corp., Norwalk, CT
105 Spiker, R.C., Pinnavaia, T.J. and Levin, J.W. (1976) Biochim. Biophys. Acta 455, 588–596
106 Smakida, A. (1966) in Applied Infrared Spectroscopy (Kendall, D.N., ed.), p. 131, Reinhold Publishing Corp., New York, NY
107 Bertz, C.P. and Ascarelli, G. (1965) Biopolymers 15, 2299–2301
108 Bertie, J.E. and Whalley, E. (1967) J. Chem. Phys. 46, 1271–1284
109 Smakida, A. (1967) Harshaw Crystal Optics, Harshaw Chemical Co.
110 Graham, J. and Wallach, D.F.H. (1969) Biochim. Biophys. Acta 193, 225–227
111 Graham, J.M. and Wallach, D.F.H. (1971) Biochim. Biophys. Acta 241, 180–194
112 Jendresiak, G.L. and Hasty, J.H. (1974) Biochim. Biophys. Acta 337, 79–91
113 Washburn, E.W. (1926) International Critical Tables, 1st edn., Vol. 1, p. 67, McGraw-Hill, New York, NY
114 Kahn, F.J. (1973) Appl. Phys. Lett. 22, 111–113
115 Powers, L. and Clark, N.A. (1975) Proc. Natl. Acad. Sci. U.S. 72, 840–843
116 Drohmer, P. (1966) in Applied Infrared Spectroscopy (Kendall, D.N., ed.), Reinhold Publishing Corporation, New York, NY

117 Avron, M. and Mateescu, Gh.-D. (1972) Infrared Spectroscopy, Wiley-Interscience, New York, NY
118 Angell, C.L. (1964) in Polarized Infrared Spectroscopy, Progess in Infrared Spectroscopy, Vol. II (Szymanski, H., ed.), F45, Plenum Press, New York, NY
119 Krohmer, P., IR Spectroscopy with Polarized Light, Perkin Elmer Corporation, Norwalk, CT
120 Chapman, D., Williams, R.M. and Ladbrooke, B.D. (1967) Chem. Phys. Lipids 1, 445–475
121 Cherry, R.J. and Morrison, A. (1966) Proc. R. Soc. London Ser. A 290, 115–142
122 Jendresiak, G.L. and Mendible, J.C. (1976) Biochim. Biophys. Acta 424, 149–158
123 Jukes, J. and Krimm, S. (1971) Spectrochim. Acta 27A, 19–34